Entanglement in an expanding toroidal Bose-Einstein condensate

Anshuman Bhardwaj,[1] Ivan Agullo,[1,2] Dimitrios Kranas,[1] Justin H. Wilson,[1] and Daniel E. Sheehy[1]
[1]*Department of Physics and Astronomy, Louisiana State University, Baton Rouge, Louisiana 70803, USA*
[2]*Perimeter Institute for Theoretical Physics 31 Caroline Street North, Waterloo, Ontario, Canada N2L 2Y5*

(Received 14 July 2023; revised 1 December 2023; accepted 14 December 2023; published 5 January 2024)

Recent experiments have employed rapidly expanding toroidal Bose-Einstein condensates (BECs) to mimic the inflationary expansion in the early universe. One expected signature of the expansion in such experiments is spontaneous particle creation (of phonons) which is observable in density-density correlations. We study entanglement of these particles, which are known to result in a two-mode squeezed state. Using techniques for Gaussian states of continuous variable systems, we quantify the entanglement generated in this system, including effects such as decoherence and the use of an initially squeezed state, which can suppress and enhance entanglement, respectively. We also describe a protocol to experimentally measure the correlations entering the covariance matrix, allowing an experimental quantification of the entanglement properties of the inflationary BEC.

DOI: 10.1103/PhysRevA.109.013305

I. INTRODUCTION

In 1966, Parker made an important discovery [1,2]: The expansion of the universe can create particles out of the vacuum (see Ref. [3] for earlier intuition about this phenomenon by Schrödinger). Parker considered Friedman-Lemaître-Robertson-Walker (FLRW) spacetimes that are asymptotically Minkowskian in the future and past, and showed that (nonconformal invariant) quantum fields that at early times are prepared in the vacuum state generically end up in an excited state. The underlying translational invariance of the gravitation field leads to momentum conservation for the quantum field, which in turn implies that particles are created in pairs, with wave numbers $\vec{k}$ and $-\vec{k}$. Phrased in a modern language, Parker showed that, for each pair $(\vec{k}, -\vec{k})$, the initial vacuum evolves to a *two-mode squeezed vacuum*, with squeezing intensity and squeezing angle determined by the expansion history of the universe. This means, in particular, that the two particles in each created pair are *entangled*.

Parker's ideas were formulated using the theory of linearized quantum fields propagating on a fixed gravitational background where the quantized fields are *test fields* which do not disrupt or modify in any way the underling geometry. This same formalism was later applied to black holes by Hawking in the mid-1970s, leading to the Hawking effect [4,5], and also to the paradigm of cosmic inflation in the early 1980s [6–12]. These two phenomena constitute important predictions of quantum field theory in curved spacetimes. In particular, the latter provides a possible explanation for the origin of the density perturbations in the early universe, which seeded the matter distribution we observe today. This would imply that the structures in our universe have emerged from a process of squeezing of the quantum vacuum. This raises the question of how to test the quantum origin of this possibility. Concretely, efforts to answer this have focused both on quantifying the genuine quantum correlations of squeezing due to inflation (i.e., measures of quantum entanglement generated) and how to observe it [13–24].

Independently, Unruh in Ref. [25] proved that the physics of quantum fields propagating on nontrivial geometries can be simulated in the laboratory, laying the groundwork for the field of analog gravity [26]. Analog models offer a test bed to recreate Parker's phenomenon of particle creation in the laboratory in a controlled manner, and to confirm its key predictions. In this paper, we focus attention on one of the simplest analog systems leading to particle creation à la Parker: a toroidal Bose-Einstein condensate (BEC) whose radius is rapidly growing. This system has been realized experimentally [27,28], and used to simulate an effectively one-dimensional inflationary universe [29–31]. These experiments observed the cosmological redshift and the damping that the expansion induces on density perturbations in the fluid. This is a promising platform to directly observe particle pair creation. Recent theory [30] has analyzed the spectrum of particles created in this system under a finite period of exponential expansion and computed the signatures that these particles produce on density-density correlation functions.

The focus of this paper is on entanglement. As mentioned above, entanglement is the quantum hallmark of the process of two-mode squeezing behind pair creation, and observing it would assist in identifying and distinguishing the physical origin of the observed correlations. Indeed, pair creation has a long history in optical and atomic physics settings, including probing the Einstein-Podolsky-Rosen paradox and Bell inequality violation using correlated photons [32–35] and the study of similar phenomena with correlated atomic beams [36–38]. The present paper builds on this theoretically, by probing the observability of the entanglement generated during the pair-creation process in an inflationary toroidal BEC. The rest of the paper is organized as follows: in Sec. II, we briefly review how the perturbations inside a rapidly expanding toroidal BEC setup lead to spontaneous creation of

phonon pairs in modes $(n, -n)$ in two-mode squeezed states (see Ref. [30] for more details). In Sec. III, we first quantify the entanglement generated in this process by using an entanglement measure (logarithmic negativity) well adapted to the physical setup. Next, this quantification allows us to analyze the way entanglement is affected by the presence of thermal noise and losses, ubiquitous in real experiments. Using the tools put forward in Refs. [39,40], we show that noise and losses *degrade* the entanglement in the final state, possibly eliminating it entirely and rendering a classical final state. Next, following the ideas in Refs. [39,40], we propose a way of amplifying the entanglement generated in this scenario, possibly compensating for the aforementioned deleterious effects. This is done by considering *stimulated* particle creation using appropriate initial states—stimulated in the standard sense of atomic physics, to be contrasted with the spontaneous effects arising when the input is merely vacuum fluctuations. In particular, we study the use of single-mode squeezed inputs as a way of stimulating additional creation of entangled pairs, increasing the observability of this effect. In Sec. IV, we propose an experimental protocol to reconstruct the final state and to measure the entanglement it contains between phonons in the mode pair $(n, -n)$. Section V provides some concluding remarks. In Appendix A, we provide details of our calculations of particle creation in an expanding toroidal BEC, in Appendix B we present a brief review of Gaussian states and entanglement measures, and in Appendix C we discuss a C^2-smooth expansion protocol for the toroidal BEC.

II. PARTICLE CREATION IN a TOROIDAL BEC

In this section, we briefly review and expand upon the work done in Ref. [30], that analyzed properties of a toroidal BEC with a time dependent radius, and the phenomenon of pair creation of phonons therein. For clarity, in Appendix A we provide additional details of the results of this section.

The system experimentally created in Refs. [27,28] is made of a BEC with toroidal shape and time dependent radius $R(t)$. In the thin-ring limit, variations in the condensate in the radial direction can be neglected, and the problem becomes effectively one-dimensional, parametrized by the angle θ. The BEC is described in terms of a complex scalar field $\hat{\Phi}(\theta, t)$ [41], which can be decomposed in terms of density $\hat{n}(\theta, t)$ and phase $\hat{\phi}(\theta, t)$:

$$\hat{\Phi}(\theta, t) = \sqrt{\hat{n}(\theta, t)}\, e^{i\hat{\phi}(\theta,t)}. \tag{1}$$

This is the Madelung representation. We are interested in *linear perturbations* $[\hat{\phi}_1(\theta, t), \hat{n}_1(\theta, t)]$ of the phase and density, respectively, over a background $[\phi_0(t), n_0(t)]$ describing the average phase and density, such that

$$\hat{\phi}(\theta, t) = \phi_0(t) + \hat{\phi}_1(\theta, t),\ \hat{n}(\theta, t) = n_0(t) + \hat{n}_1(\theta, t). \tag{2}$$

The canonical commutation relation of the condensate $\hat{\Phi}$ implies that $(\hat{n}_1, \hat{\phi}_1)$ form a canonical operator pair. The quantization of the pair $(\hat{n}_1, \hat{\phi}_1)$ is standard [30]. We begin with an expansion of these operators in terms of annihilation and creation operators $(\hat{a}_n, \hat{a}_n^\dagger)$:

$$\hat{\phi}_1(\theta, t) = \sqrt{\frac{U}{2\pi \mathcal{V}_0 \hbar}} \sum_{n=-\infty}^{\infty} [e^{in\theta}\, \chi_n(t)\, \hat{a}_n + \text{H.c.}], \tag{3a}$$

$$\hat{n}_1(\theta, t) = \sqrt{\frac{U\mathcal{V}_0}{2\pi \hbar}} \sum_{n=-\infty}^{\infty} [e^{in\theta}\, \eta_n(t) \hat{a}_n + \text{H.c.}], \tag{3b}$$

where H.c. indicates the Hermitian conjugate, $U = \frac{4\pi a_s \hbar^2}{M}$ is the interaction parameter with a_s being the scattering length, M is the mass of the atoms in the condensate, $2\pi\mathcal{V}(t)$ is the volume of the condensate, and $\mathcal{V}_0 \equiv \mathcal{V}(0)$. The time dependent functions $\chi_n(t)$ are the mode functions, and they form a basis of the vector space of complex solutions to the equations of motion [30]

$$\ddot{\chi}_n + (1+\gamma)\frac{\dot{R}}{R}\dot{\chi}_n + \alpha\, \frac{n^2 c^2}{R^2}\chi_n = 0. \tag{4}$$

The steps leading to Eq. (4), provided in detail in Appendix A, involve expressing the equations of motion for $\hat{\phi}_1(\theta, t)$ and $\hat{n}_1(\theta, t)$ as equations of motion for $\chi_n(t)$ and $\eta_n(t)$ via Eqs. (3). Combining the latter and applying approximations relevant to the toroidal geometry then leads to Eq. (4). In these equations, that are analogous to the Mukhanov-Sasaki equations [42–44] from cosmology, c is the wave speed and γ and α are corrections due to quantum pressure coming from the boson kinetic energy in the original system Hamiltonian which we shall take to be constants, although they generally depend on the density, the radius of the ring, and the mode index. As discussed in Ref. [30] and Appendix A, realistic values for the latter parameters are $\gamma \simeq 0.1$ (close to zero) and $\alpha \simeq 1$. For simplicity, we take $\alpha = 1$ (equivalent to absorbing it into c) and, since particle production only occurs for nonzero γ, we generally assume $0 < \gamma < 1$.

Let us write the time dependent radius of the toroid as $R(t) = R_0\, a(t)$, with R_0 being a constant. Then, if the mode functions are chosen to be normalized such that $(\chi_n \dot{\chi}_n^* - \chi_n^* \dot{\chi}_n) = i\, a(t)^{-(1+\gamma)}$ for all n at any instant, then this normalization is preserved throughout the evolution. Furthermore, $\hat{a}_n$ and $\hat{a}_n^\dagger$ in (3) satisfy the algebra of creation and annihilation operators, i.e., $[\hat{a}_n, \hat{a}_{n'}^\dagger] = \delta_{nn'}$ and $[\hat{a}_n, \hat{a}_{n'}] = 0$.

Notably, Eqs. (3) and (4) are formally analogs to the equations describing the propagation of a scalar field in a spatially flat FLRW universe, with scale factor $a(t)$.[1] Hence, the system under consideration makes it possible to recreate the physics of quantum fields propagating in an expanding universe, by appropriately engineering a time dependent radius $R(t)$ of the toroidal BEC, as was done in Refs. [27,28].

Following the experimental platform described in Refs. [27,28], we consider $R(t)$ that is time independent

[1] If the quantum pressure γ were to vanish, Eq. (4) would be equivalent to the equation one would find for the modes of a massless, minimally coupled scalar field in a FLRW spacetime with one spatial dimension. But such a field is conformally invariant, and since the FLRW geometry is conformally flat, there would be no particle creation in that situation. The presence of $\gamma \neq 0$ in (4) breaks conformal invariance and makes it possible for phonon pair creation to occur.

in the past, then varies monotonically, and finally becomes constant again. These early- and late-time regions where $R(t)$ is time independent are the "in" and "out" regions, respectively, in which the system is stationary and there is a well-defined notion of ground state—the in and out vacuum, $|0_{\rm in}\rangle$ and $|0_{\rm out}\rangle$, respectively—each associated with a set of annihilation and creation operators, which we will denote as $(\hat{a}^{(\rm in)}, \hat{a}^{(\rm in)\dagger})$ and $(\hat{a}^{(\rm out)}, \hat{a}^{(\rm out)\dagger})$, respectively. (If nonexpanding in and out regions were absent, it would be necessary to make a choice of specific initial and final creation and annihilation operators. The calculation of the particles and entanglement generated by the expansion would then rely on this choice.)

One question of interest is the following: if the condensate is prepared in the mean-field ground state at early times, what is the state at late times? The answer to this question is well known [1,2,30]:

$$\hat{U}\,|0_{\rm in}\rangle = \prod_{n\in\mathcal{Z}} \frac{1}{\sqrt{|\alpha_n|}} e^{\frac{\beta_n^*}{2\alpha_n^*}\hat{a}_n^{(\rm out)\dagger}\hat{a}_{-n}^{(\rm out)\dagger}}\,|0_{\rm out}\rangle, \tag{5}$$

where $\hat{U}$ is the time-evolution operator, and α_n and β_n are the Bogoliubov coefficients relating the in and out creation and annihilation operators:

$$\hat{a}_n^{(\rm out)} = \alpha_n\,\hat{a}_n^{(\rm in)} + \beta_n^*\,\hat{a}_{-n}^{(\rm in)\dagger}. \tag{6}$$

By expanding the exponential in (5), we see that the result of evolving the in vacuum produces a state at late times that is made of linear combinations of states of the form $(\hat{a}_n^{(\rm out)\dagger}\hat{a}_{-n}^{(\rm out)\dagger})^N|0_{\rm out}\rangle$. These states contain $2N$ phonons, half of them with label n and the other half with label $-n$. This implies that phonons are created in pairs $(n, -n)$. Since modes with label n and $-n$ describe counter- and clockwise propagating plane waves, respectively, the creation of these pairs respects angular momentum conservation. Furthermore, it is not difficult to check that there are $|\beta_n|^2$ phonons, on average, in the mode n at late times. In the next section, we will write the final state in a different form, which will make manifest that (5) is a Gaussian state resulting by applying a process of two-mode squeezing to the vacuum for each pair $(n, -n)$, and we will describe a way of quantifying the entanglement in this state.

Our next task is to choose a specific function for the toroidal BEC radius $R(t)$ entering Eq. (4). Following Ref. [30], we choose

$$R(t) = \begin{cases} R_0, & \text{for } t < 0, \\ R_0 e^{t/\tau}, & \text{for } 0 < t < t_f, \\ R_0 e^{t_f/\tau}, & \text{for } t > t_f. \end{cases} \tag{7}$$

Thus, for early times $t < 0$, the radius is a constant R_0, with the exponential expansion beginning at $t = 0$. In this exponential regime, we can write $R(t) = R_0\,a(t)$ with $a(t) = e^{t/\tau}$ being the scale factor, thereby mimicking an inflationary universe, where the constant τ plays the role of the "Hubble time." For later times $t > t_f$, the radius is again a constant $R_f = R_0 e^{t_f/\tau}$.

It is important to emphasize that the conceptual analysis and the tools presented in this paper are applicable to any form of the expansion history $R(t)$. We use the simple expression (7) merely for illustrative purposes. All the plots shown below can be straightforwardly recomputed for $R(t)$ adapted to concrete experimental platforms.

The simplicity of this choice leads to an issue: the function $R(t)$ in Eq. (7) is continuous but not differentiable at $t = 0$ and t_f. We expect that, in a real experiment, the ramp up and down will be smoother (with its own timescale), and as a result, this abrupt model expansion we include here may lead to spurious particle production outside of the central inflationary regime. This issue was pointed out by Glenz and Parker (GP), who argued that such artifacts can be avoided as long as $R(t)$ is at least C^2 [45]. The experiments of Refs. [27,28] use an error-function profile for the trap expansion to minimize such slope discontinuities.

To justify our use of Eq. (7) despite this issue, we note that, as emphasized by GP, artifacts of a C^0 scale factor are most significant at large mode index, i.e., density fluctuations at short distances. We argue that, since such high mode indices are probably inaccessible to real toroidal BEC experiments, Eq. (7) is sufficient for our goal of studying entanglement of particle production. In addition, Eq. (7) has the advantage of providing closed analytic expressions for the Bogoliubov coefficients α_n and β_n [30].

Nevertheless, for completeness, in Appendix C we consider an expansion history $R(t)$ of differentiability class C^2, also containing an inflationary period. There, we show that the resulting mean number of created quanta $|\beta_n|^2$ behaves universally as $n^{-\gamma}$ for sufficiently large n, directly reflecting the dissipative role of the quantum pressure γ in the equation of motion (4).

Now returning to our model Eq. (7) for the BEC radius, we quote the resulting Bogoliubov coefficients [30]:

$$\alpha_n = \frac{1}{2}\frac{e^{-\frac{t_f}{2\tau}}}{J_{\frac{1+\gamma}{2}}(z_0)J_{\frac{1-\gamma}{2}}(z_0) + J_{-\frac{1+\gamma}{2}}(z_0)J_{\frac{-1+\gamma}{2}}(z_0)} \times\Big[\Big\{J_{\frac{1-\gamma}{2}}(z_0) + iJ_{-\frac{1+\gamma}{2}}(z_0)\Big\}\Big\{J_{\frac{1+\gamma}{2}}(z_f) - iJ_{\frac{-1+\gamma}{2}}(z_f)\Big\} + \Big\{J_{\frac{-1+\gamma}{2}}(z_0) - iJ_{\frac{1+\gamma}{2}}(z_0)\Big\}\Big\{J_{-\frac{1+\gamma}{2}}(z_f) + iJ_{\frac{1-\gamma}{2}}(z_f)\Big\}\Big], \tag{8}$$

$$\beta_n = \frac{1}{2}\frac{e^{-\frac{t_f}{2\tau}}}{J_{\frac{1+\gamma}{2}}(z_0)J_{\frac{1-\gamma}{2}}(z_0) + J_{-\frac{1+\gamma}{2}}(z_0)J_{\frac{-1+\gamma}{2}}(z_0)} \times\Big[\Big\{J_{\frac{1-\gamma}{2}}(z_0) + iJ_{-\frac{1+\gamma}{2}}(z_0)\Big\}\Big\{J_{\frac{1+\gamma}{2}}(z_f) + iJ_{\frac{-1+\gamma}{2}}(z_f)\Big\} + \Big\{J_{\frac{-1+\gamma}{2}}(z_0) - iJ_{\frac{1+\gamma}{2}}(z_0)\Big\}\Big\{J_{-\frac{1+\gamma}{2}}(z_f) - iJ_{\frac{1-\gamma}{2}}(z_f)\Big\}\Big], \tag{9}$$

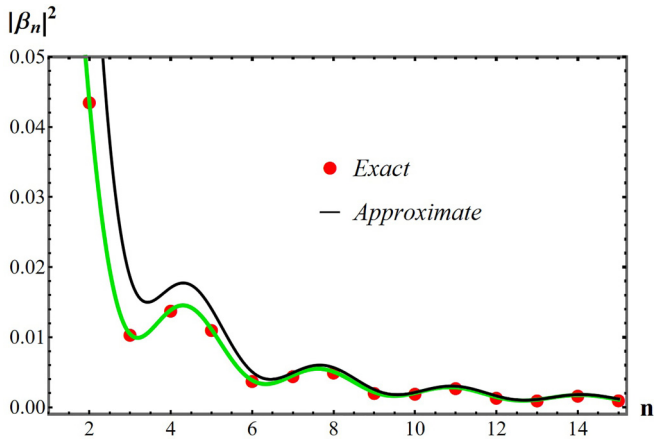

FIG. 1. Plot of the mean number of quanta $|\beta_n|^2$ created in mode n. The red circles indicate the exact theoretical result from the absolute value squared of Eq. (9), and the black curve shows the approximate result in Eq. (10), valid in the limit of small γ and large n. The green curve shows $|\beta_n|^2$ as a continuous function to emphasize its overall dependence on the discrete mode indices. For this plot, we took the quantum pressure to be $\gamma = 0.5$, the speed of sound to be $c = 2/\text{s}$, the initial radius to be $R_0 = 10\,\mu\text{m}$, the expansion timescale to be $\tau = 6.21$, and the duration of expansion to be $t_f = 10$.

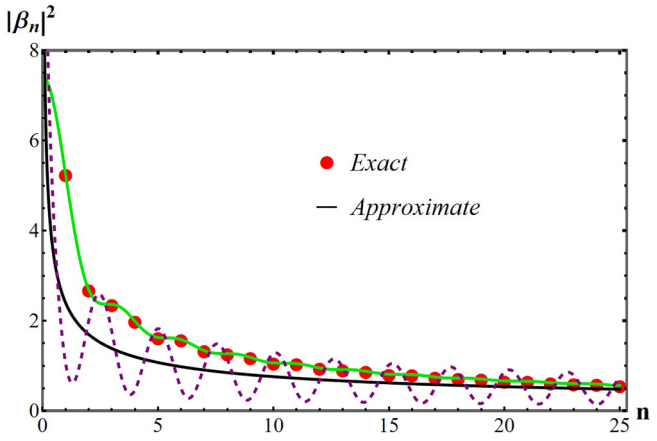

FIG. 2. Plot of the mean number of quanta $|\beta_n|^2$ created in mode n. The red circles indicate the exact theoretical result from the absolute value squared of Eq. (9), and the green curve is its continuous version to emphasize its overall dependence on the discrete mode indices. We compare this with the dashed purple curve that shows the approximate result in Eq. (11), where the black curve is obtained by averaging the two cosine square terms in (11). For this plot, we took the same parameters as Fig. 1, but with a much longer expansion time $t_f = 1 \times 10^4$.

where $J_n(x)$ are Bessel functions of the first kind, and we define parameters $z_0 \equiv \frac{|n|c\tau}{R_0}$ and $z_f \equiv \frac{|n|c\tau}{R_f}$.

Next, we examine various limits for the particle production $|\beta_n|^2$. A simple approximation for $|\beta_n|^2$ (valid in the limit $\gamma \ll 1$ and $n \gg 1$) is given by Ref. [30]

$$|\beta_n|^2 \approx \frac{1}{n^2}\left(\frac{\gamma}{4}\right)^2\left(\frac{c\tau}{R_0}\right)^{-2}\left[1 + a_f^2 - 2a_f\cos(2n\theta_{\text{H}})\right], \quad (10)$$

where $a_f = e^{\frac{t_f}{\tau}}$ is the ratio of final and initial radii R_f/R_0, and $\theta_{\text{H}} = \frac{c\tau}{R_0}(1 - a_f^{-1})$ is the angular horizon size at the end of the expansion. Although this approximation is obtained as a large n limit, it is quite accurate for $n \gtrsim 3$ in relevant parameter ranges as can be seen in Fig. 1. The parameters chosen in this figure, and elsewhere in the paper, are approximately based on the experiments of Ref. [27], as discussed in Ref. [30], although below we also explore how phenomena change with these parameters. This approximation makes it clear that oscillations in the particle creation number shown in Fig. 1 reflect the value of the angular size of the Hubble horizon θ_{H} (see Ref. [30] for details). Note also that the pair creation in the expanding ring does not produce a particle distribution with a blackbody spectrum, as happens for analog models for which causal horizons are present.

We can still recover the inflationary regime $|\beta_n|^2 \sim n^{-\gamma}$ with assumptions which simplify the Bessel functions with arguments z_0 and z_f in Eq. (9). First, we assume that the modes n are initially well within the horizon. In this limit, $z_0 \to \infty$, and the Bessel functions with argument z_0 become $J_\alpha(z_0) \sim \sqrt{\frac{2}{\pi z_0}}\cos(z_0 - \frac{\alpha\pi}{2} - \frac{\pi}{4})$. Second, if we assume that the toroid expands for a very long time (an experimentally challenging assumption) the modes n exit the horizon and attain very large wavelengths compared to the horizon size, i.e., $R_f/n \gg c\tau$, and the Bessel functions with argument z_f become $J_\alpha(z_f) \sim \frac{1}{\Gamma(\alpha+1)}(\frac{z_f}{2})^\alpha$. In this regime, the particle creation number in Eq. (9) takes the following form:

$$|\beta_n|^2 \approx \frac{\pi}{4}\left(\frac{R_f}{2c\tau}\right)^\gamma \frac{\cos^2\left(z_0 - \frac{\pi\gamma}{4}\right) + \cos^2\left(z_0 + \frac{\pi\gamma}{4}\right)}{\sin^2\left(\frac{1+\gamma}{2}\pi\right)\Gamma^2\left(\frac{1+\gamma}{2}\right)}\, n^{-\gamma}. \quad (11)$$

As can be seen from Fig. 2, this approximation fits well with the exact expression for $|\beta_n|^2$ for large expansion times, leading to the universal behavior of $n^{-\gamma}$ as predicted by GP [45]. However, for smaller expansion times (where R_f is not so large), it is more appropriate to use the n^{-2} asymptotic form in Eq. (10). In addition to being experimentally challenging, long expansions lead to an increase in the coherence length[2] and a decrease of the ring width with increasing time, to the point that the hydrodynamic limit (which requires the mode wavelength to be large compared to the coherence length) is violated. Intuitively, long expansion times decrease the density to a point where individual atoms are spread out sufficiently that they cannot interact and form the coherent mean-field ground state.

The preceding two regimes of the particle creation number, Eqs. (10) and (11), approximately hold in the regimes $n \gg \frac{R_f}{c\tau}$ and $\frac{R_0}{c\tau} \ll n \ll \frac{R_f}{c\tau}$, respectively. The crossover between these two regimes can be clearly seen in a log-log plot of $|\beta_n|^2$ vs n, as shown in Fig. 3. In the third regime of $n \ll \frac{R_0}{c\tau}$, $|\beta_n|^2$ is approximately independent of mode index. In Ref. [30], it was shown that the pair creation represented by $|\beta_n|^2$ produces

[2]For a BEC, the coherence length is defined as the length scale over which the condensate maintains coherence in its density given by $\xi = \frac{\hbar}{\sqrt{2}Mc}$, where M is the mass of the bosonic atoms and c is the speed of sound.

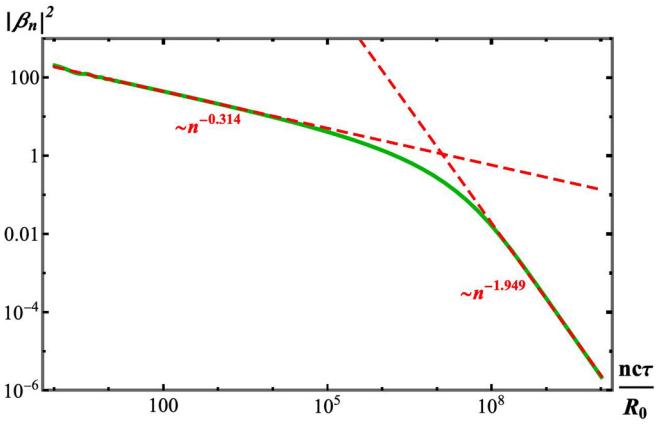

FIG. 3. Log-log plot of the mean number of quanta $|\beta_n|^2$ created in mode n, for the case of $e^{t_f/\tau} = 10^8$ and $\gamma = 0.3$ (solid green curve). The red dashed lines are linear fits with the fitted power law shown on the plot, showing that $|\beta_n|^2$ indeed approximately exhibits n^{-2} behavior at large n and $n^{-\gamma}$ behavior at smaller n, consistent with Eqs. (10) and (11), respectively.

distinctive features in density-density correlations of the condensate, which could be observed in the laboratory. The main effect is a kinklike feature in the density-density two-point correlation function, located at an angular separation determined by the angular size of the horizon $\theta_{\rm H}$. The amplitude of this kink increases with increasing quantum pressure and BEC temperature. In the zero-temperature limit, the kink degenerates into a "cusp"-like feature.

Having described both the perturbations in an expanding toroidal BEC and how such expansion leads to spontaneous phonon pair creation in a two-mode squeezed state (5) determined by β_n given in Eq. (9), we are ready to discuss the entanglement of these phonon pairs, i.e., how to quantify it and what factors lead to its degradation and enhancement.

III. ENTANGLEMENT

In this section, we reformulate the evolution of phonon perturbations propagating in the expanding toroidal BEC, using the language of continuous variable quantum systems and Gaussian states [46] (see Ref. [40] for applications to analog gravity). This formalism is useful because the equations of motion (4) of phonon perturbations are linear, and therefore preserve the Gaussianity of the quantum states.

Using this language, the evolution of phonon perturbations is described by a collection of two-mode squeezers, each acting on a pair $(n, -n)$ of modes. Classically, a two-mode squeezer represents a non-energy-conserving process, able to amplify (or damp) waves. Quantum mechanics adds two key features. On the one hand, even the vacuum can be amplified. On the other hand, the amplification process creates pairwise entanglement between quanta. The formalism used in this section provides an efficient toolbox to quantify this entanglement.

Gaussian states include vacua, coherent, thermal, and squeezed states. Therefore, although our analysis is restricted, the family of Gaussian states is sufficiently general to approximately describe most of the states one can create and manipulate in the laboratory.

A. Evolution: Two-mode squeezers and pair creation

The background condensate (described by n_0 and ϕ_0) is homogenous, in the sense that neither n_0 nor ϕ_0 depends on the location θ along the ring. Consequently, the evolution of condensate perturbations $\chi(\theta, t)$ is such that Fourier modes with spatial dependence $e^{-in\theta}$, $n \in \mathbb{Z}$, evolve independently of each other. This is manifest in Eq. (4). For a fixed n, there are only two modes with such spatial dependence, namely χ_n and χ^*_{-n}, using the notation introduced in the previous section. Hence, the evolution of the perturbations factors out in the evolution of pairs $(n, -n)$ of modes, with no interaction among different pairs. Since each pair corresponds to a quantum-mechanical linear system with two degrees of freedom, we can apply the formalism summarized in Appendix B (we refer the reader to this Appendix for details omitted here).

Let $\hat{\mathbf{A}}_n^{(\rm in)}$ be the (column) vector of in creation and annihilation operators for a pair $(n, -n)$ of modes

$$\hat{\mathbf{A}}_n^{(\rm in)} \equiv \left(\hat{a}_n^{(\rm in)}, \hat{a}_n^{(\rm in)\dagger}, \hat{a}_{-n}^{(\rm in)}, \hat{a}_{-n}^{(\rm in)\dagger}\right)^\top, \tag{12}$$

and let $\hat{\mathbf{A}}_n^{(\rm out)}$ be similarly defined for the out modes. Expression (6) above implies that the matrix $\mathbf{S}_{(\mathbf{A},n)}$ describing the in-out scattering process, $\hat{\mathbf{A}}_n^{(\rm out)} = \mathbf{S}_{(\mathbf{A},n)} \cdot \hat{\mathbf{A}}_n^{(\rm in)}$, is

$$\mathbf{S}_{(\mathbf{A},n)} = \begin{bmatrix} \alpha_n & 0 & 0 & \beta_n^* \\ 0 & \alpha_n^* & \beta_n & 0 \\ 0 & \beta_n^* & \alpha_n & 0 \\ \beta_n & 0 & 0 & \alpha_n^* \end{bmatrix}. \tag{13}$$

This is precisely the form of a *two-mode squeezer* (see, e.g., Appendix A of Ref. [40] for a short summary of this type of symplectic transformation). From $\mathbf{S}_{(\mathbf{A},n)}$, we can obtain the scattering matrix $\mathbf{S}_n$ describing the evolution of canonical pairs

$$\hat{x}_n = \frac{1}{\sqrt{2}}(\hat{a}_n + \hat{a}_n^\dagger), \tag{14a}$$

$$\hat{p}_n = -\frac{i}{\sqrt{2}}(\hat{a}_n - \hat{a}_n^\dagger), \tag{14b}$$

by simple multiplication with the "change of basis matrix" $\mathbf{B}$, $\mathbf{S}_n = \mathbf{B} \cdot \mathbf{S}_{(\mathbf{A},n)} \cdot (\mathbf{B})^{-1}$, where $\mathbf{B}$ is written in Eq. (B5) of Appendix B.

In experimental settings, the initial state of the system is well approximated by a thermal state in equilibrium with the environment at temperature T. This is a mixed Gaussian state, which means it is completely determined by its first ($\boldsymbol{\mu}$) and second ($\boldsymbol{\sigma}$) moments, with the latter being termed the covariance matrix. [See Appendix B, where these are defined in Eqs. (B9) and (B10), respectively.] In the present case, we find

$$\boldsymbol{\mu}_{(n)}^{(\rm in)} = (0, 0, 0, 0)^\top, \tag{15}$$

$$\boldsymbol{\sigma}_{(n)}^{(\rm in)} = [1 + 2n_B(E_n)]\,\mathbb{I}_4, \tag{16}$$

where $\mathbb{I}_4$ is the identity matrix and $n_{\rm B}(x) = (e^{\beta x} - 1)^{-1}$ is the mean number of thermal quanta, given by the

Bose-Einstein distribution with $\beta = (k_B T)^{-1}$, and k_B the Boltzmann constant. Here, the Bogoliubov energy dispersion is $E_n = \sqrt{\epsilon_n(\epsilon_n + 2Mc^2)}$, where c is the speed of sound and $\epsilon_n = \frac{\hbar^2 n^2}{2MR^2}$ is the single-particle energy in the toroid. In the hydrodynamic limit of interest here, in which the mode wavelength is large compared to the coherence length, we approximate $E_n \simeq \frac{\hbar c}{R}|n|$. From this, we obtain the final state, which is again Gaussian and described by

$$\boldsymbol{\mu}^{(\text{out})}_{(n)} = \mathbf{S}_n \cdot \boldsymbol{\mu}^{(\text{in})}_{(n)} = (0,0,0,0)^\top,$$
$$\boldsymbol{\sigma}^{(\text{out})}_{(n)} = \mathbf{S}_n \cdot \boldsymbol{\sigma}^{(\text{in})}_{(n)} \cdot \mathbf{S}_n^\top = (1+2n_B)\begin{bmatrix} |\alpha_n|^2+|\beta_n|^2 & 0 & \alpha_n^*\beta_n+\alpha_n\beta_n^* & i(\alpha_n^*\beta_n-\alpha_n\beta_n^*) \\ 0 & |\alpha_n|^2+|\beta_n|^2 & i(\alpha_n^*\beta_n-\alpha_n\beta_n^*) & -(\alpha_n^*\beta_n+\alpha_n\beta_n^*) \\ \alpha_n^*\beta_n+\alpha_n\beta_n^* & i(\alpha_n^*\beta_n-\alpha_n\beta_n^*) & |\alpha_n|^2+|\beta_n|^2 & 0 \\ i(\alpha_n^*\beta_n-\alpha_n\beta_n^*) & -(\alpha_n^*\beta_n+\alpha_n\beta_n^*) & 0 & |\alpha_n|^2+|\beta_n|^2 \end{bmatrix}. \quad (17)$$

Note the Bogoliubov coefficients α_n and β_n were written in Eqs. (8) and (9) above for the dynamical expansion given by Eq. (7). Here and below we have suppressed the argument of the Bose-Einstein distribution, which is always E_n. This covariance matrix is of the form

$$\boldsymbol{\sigma}^{(\text{out})}_{(n)} = \begin{bmatrix} \boldsymbol{\sigma}^{(\text{red})}_{(n)} & \mathbf{C}_{(n)} \\ \mathbf{C}^\top_{(n)} & \boldsymbol{\sigma}^{(\text{red})}_{(-n)} \end{bmatrix}, \quad (18)$$

where $\boldsymbol{\sigma}^{(\text{red})}_{(n)}$ and $\boldsymbol{\sigma}^{(\text{red})}_{(-n)}$ are the covariance matrices of the reduced state describing the modes n and $-n$, respectively, which are equal to each other. The matrix $\mathbf{C}_{(n)}$ encodes the correlations between these two modes. We will see in the next section that these correlations contain entanglement for sufficiently low environment temperatures.

From Eq. (17), we extract all predictions about the final state such as the mean number of phonons in one of the two modes, say the mode n:

$$\langle \hat{N}_n \rangle = \frac{1}{4}\text{Tr}\{\boldsymbol{\sigma}^{(\text{red})}_{(n)}\} + \frac{1}{2}\left(\boldsymbol{\mu}^{(\text{red})}_{(n)}\right)^\top \boldsymbol{\mu}^{(\text{red})}_{(n)} - \frac{1}{2}, \quad (19)$$

where

$$\boldsymbol{\mu}^{(\text{red})}_{(n)} = (0,0),$$
$$\boldsymbol{\sigma}^{(\text{red})}_{(n)} = (1+2n_B)\left(|\alpha_n|^2+|\beta_n|^2\right)\mathbb{I}_2 \quad (20)$$

are the first moments and covariance matrix of the reduced state describing the mode n alone. We obtain

$$\langle \hat{N}_n \rangle = \tfrac{1}{2}[(1+2n_B)\left(|\alpha_n|^2+|\beta_n|^2\right) - 1] \quad (21)$$
$$= n_B + |\beta_n|^2 + 2n_B|\beta_n|^2, \quad (22)$$

where in the second line we have used the identity $|\alpha_n|^2 - |\beta_n|^2 = 1$. This last expression offers a simple interpretation. On the one hand, we see that, in the zero-temperature limit, $n_B \to 0$, we obtain $\langle \hat{N}_n \rangle = |\beta_n|^2$, as expected. For finite temperature, $\langle \hat{N}_{|n|} \rangle$ has three contributions. The first one, given by n_B, simply corresponds to the thermal quanta already present in the initial state. The second term, $|\beta_n|^2$, corresponds to the quanta created from the vacuum. The third term contains the product $n_B|\beta_n|^2$, which has the interpretation of *stimulated or induced phonon creation* (i.e., the mere presence of initial quanta induces further pair creation).

The number of quanta in the mode $-n$ has exactly the same value, in such a way that $\langle \hat{N}_n \rangle - \langle \hat{N}_{-n} \rangle$ remains constant in the course of time. In other words, quanta are created in pairs $(n, -n)$.

B. Entanglement

In this subsection, we investigate under what conditions the out state written in Eq. (17) for the $(n, -n)$ pair is entangled. Appendix B contains a summary of a few ways of answering this question (see Ref. [46] for further details on entanglement measures for Gaussian states; see also Refs. [39,40] for applications to Hawking radiation).

The state (17) is a mixed state for any nonzero environment temperature T. This can be seen by computing the purity of the state, which, as summarized in Appendix B, is equal to $P(\boldsymbol{\sigma}^{(\text{out})}_{(n)}) = 1/\sqrt{\det \boldsymbol{\sigma}^{(\text{out})}_{(n)}}$. A quick calculation produces $P(\boldsymbol{\sigma}^{(\text{out})}_{(n)}) = (1+2n_B)^{-2}$. The mixed nature of the out state (17) implies, in particular, that entanglement entropy (which quantifies entanglement only when the state of the total system is pure) is not an appropriate measure to quantify the entanglement between modes $(n, -n)$.

Instead, we use logarithmic negativity ($E_{\mathcal{N}}$), defined in Appendix B, which is based on the Peres-Horodecki or positivity of the partial transpose (PPT) criterion [47–49]. For Gaussian states, $E_{\mathcal{N}}$ can be computed from the symplectic eigenvalues of the "partially transposed" covariance matrix. Furthermore, for the systems we are interested in here—single-mode subsystems and Gaussian states—$E_{\mathcal{N}}$ is a faithful entanglement quantifier, in the sense that $E_{\mathcal{N}}$ is different from zero *if and only if* the state is entangled. It is also an entanglement monotone—higher $E_{\mathcal{N}}$ means more entanglement. $E_{\mathcal{N}}$ is measured in entangled bits (ebits), defined as the amount of entanglement contained in a Bell pair.

Applying expression (B17) to the state (17), we obtain

$$E_{\mathcal{N}}[n] = \max(0, -\log_2[(1+2n_B)(|\alpha_n| - |\beta_n|)^2])$$
$$= \max(0, -\log_2[(1+2n_B)(\sqrt{1+|\beta_n|^2} - |\beta_n|)^2)], \quad (23)$$

where we have used the identity $|\alpha_n|^2 - |\beta_n|^2 = 1$ in the last equality. Note that the argument of the logarithm here is the minimum symplectic eigenvalue of the partially transposed covariance matrix.

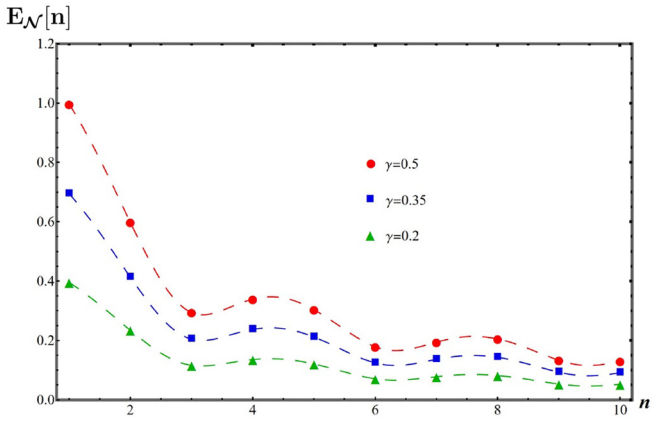

FIG. 4. Logarithmic negativity between phonons labeled by n and $-n$, for zero ambient temperature $T = 0$, for three values of the quantum pressure parameter: $\gamma = 0.2$ (*green triangles*), $\gamma = 0.35$ (*blue squares*), and $\gamma = 0.5$ (*red circles*). The mode index n is discrete; we have added a continuous dashed line to increase the visibility of the overall dependence of $E_{\mathcal{N}}$ with n. For this plot, all other parameters are the same as in Fig. 1

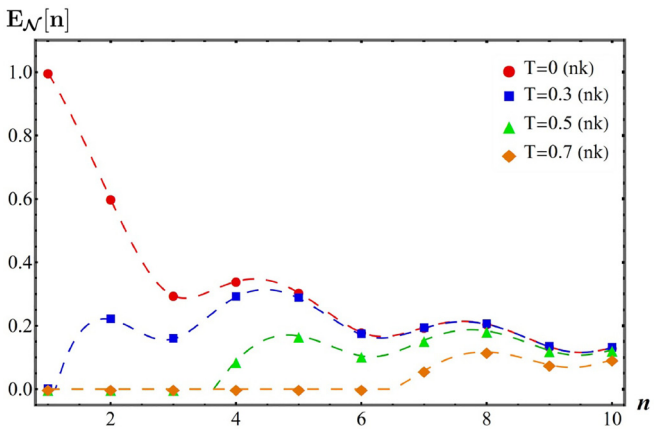

FIG. 5. Logarithmic negativity $E_{\mathcal{N}}[n]$ vs the mode index n, for various values of the environment temperature, $T = 0$ nK (*red circles*), $T = 0.3$ nK (*blue squares*), $T = 0.5$ nK (*green triangles*), and $T = 0.7$ nK (*orange diamonds*). The figure shows that entanglement in the final state is degraded by ambient thermal noise, and that the entanglement in pairs with small n is more fragile. For this plot, we use quantum pressure $\gamma = 0.5$, with all other parameters being the same as in Fig. 1.

We first discuss the situation in which the ambient temperature is zero. Substituting $n_B = 0$ in Eq. (23), we obtain $E_{\mathcal{N}}[n] = \text{Max}(0, -\log_2[(\sqrt{1+|\beta_n|^2} - |\beta_n|)^2)]$. This expression is equal to zero if and only if $\beta_n = 0$, and grows monotonically with β_n. This result tells us, on the one hand, that the members within each created phonon pair are entangled. Furthermore, since, for $T = 0$, $|\beta_n|^2$ is equal to the number of pairs created, the total entanglement grows monotonically with the number of pairs created. Figure 4 shows $E_{\mathcal{N}}$ vs the mode index n, for the expansion history given in (7), where we can recognize the shape of $|\beta_n|^2$ shown in Fig. 1, namely a rapid falloff with increasing n and oscillations dictated by the angular size of the horizon.

The second important lesson from expression (23) is the effect of ambient thermal noise on the generation of entanglement. This expression tells us that $E_{\mathcal{N}}$ is zero when the argument of the logarithm is larger than 1. The effect of thermal noise is to add the factor $(1 + 2n_B)$ (recall, n_B is the mean number of thermal quanta). This factor is larger than 1, and we can always make $E_{\mathcal{N}}$ equal to zero by increasing n_B. In other words, *thermal noise degrades the entanglement between modes n and* $-n$, even making it disappear completely above a threshold temperature, which we will denote by $T_v(n)$. The value of this critical temperature can be easily obtained from expression (23), by writing n_B in terms of $T_v(n)$. We obtain[3]

$$T_v(n) = \frac{E_n}{k_B}\left[\ln\left\{1 + \frac{1}{|\beta_n|(|\beta_n| + \sqrt{1+|\beta_n|})}\right\}\right]^{-1}. \quad (24)$$

The interpretation of this expression is simple: when thermal noisy phonon quanta dominate over the quanta created by the expansion, the entanglement in the pair $(n, -n)$ vanishes. In other words, the entanglement in the final state results from a competition between the pair creation and the environmental noise. But recall that the number of created pairs is dictated by $|\beta_n|^2$, which falls off approximately as n^{-2}, while the number of thermal quanta n_B falls exponentially fast with n. Hence, thermal noise will degrade more easily the entanglement in pairs with lower value of the mode index n. Indeed, this is shown in Fig. 5, where we plot $E_{\mathcal{N}}$ vs n for different ambient temperatures, showing that $E_{\mathcal{N}}[n]$ is more strongly suppressed at small mode index n. This behavior is also exhibited in Fig. 6, which shows the threshold temperature T_v at which $E_{\mathcal{N}}[n]$ approximately increases (with small oscillations) with

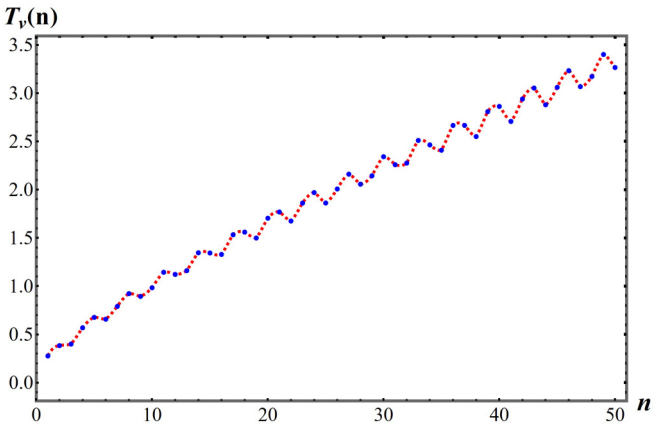

FIG. 6. Critical temperature $T_v(n)$ (in nK) at which the entanglement in the mode pair $(n, -n)$ completely vanishes. The blue dots represent the data for each mode index and the continuous red dashed line shows the overall dependence of T_v with n. Larger ambient temperature is needed to degrade the entanglement in pairs with large mode index n. The oscillations originate in the oscillatory character of $|\beta_n|^2$. For this figure, we consider the same parameters as in Fig. 5.

[3]The same result for $T_v(n)$ can be obtained from the Bell-like inequality $\Delta < 0$, with Δ defined in Eq. (B18), as explained in Appendix B.

increasing n. We emphasize again that, while the method is general, the results plotted in Figs. 4–6 apply specifically to the expansion history (7).

In summary, in the idealized situation of no initial density fluctuations, the spontaneous phonon-pair creation comes together with the generation of entanglement. We find that the presence of thermal noise drastically changes this picture. The stimulated pair creation dominates over the spontaneous emission. On the other hand, thermal noise degrades the entanglement in the final state, rendering the state classical. The expressions derived in this section quantify these quantum effects and their degradation.

C. Losses and efficiency

The discussion until now assumes an ideal situation where the process of expansion is a quantum channel with no losses. Thus, there is no decoherence, and the probes used to detect perturbations in the final static BEC have perfect efficiency. Losses and inefficiencies are, however, ubiquitous in realistic situations, and the goal of this section is to quantify the effects they have on the quantum coherence of the final state using a simple model.

A simple yet useful model is provided by the so-called quantum attenuator channel (see, e.g., Ref. [46]) characterized by a loss factor $\eta \in (0, 1)$. This is a Gaussian channel, in the sense that the Gaussianity of the state is preserved. More concretely, the channel transforms the final state as

$$\left(\boldsymbol{\mu}_{(n)}^{(\mathrm{out})}, \boldsymbol{\sigma}_{(n)}^{(\mathrm{out})}\right) \to \left(\sqrt{\eta}\,\boldsymbol{\mu}_{(n)}^{(\mathrm{out})},\ \eta\,\boldsymbol{\sigma}_{(n)}^{\mathrm{out}} + (1-\eta)\,\mathbb{I}_4\right). \quad (25)$$

Simply, quanta are detected with probability η or are otherwise lost ($\eta = 1$ corresponds to the ideal situation discussed above). Following previous sections, we can reevaluate the logarithmic negativity $E_{\mathcal{N}}[n]$ for a pair of modes $(n, -n)$ and quantify entanglement in the final state after losses and/or inefficiencies. We obtain

$$E_{\mathcal{N}}[n] = \max(0, -\log_2 \nu_{\mathrm{T},\eta}[n]) \quad (26)$$

where

$$\nu_{\mathrm{T},\eta}[n] = \frac{1}{4\sqrt{2}}\sqrt{X - \sqrt{Y}}, \quad \text{with}$$

$$\begin{aligned} X = {} & 16[2(1-\eta)^2 + 2(1+2n_{\mathrm{B}})^2\eta^2(|\alpha_n|^4 + |\beta_n|^4) \\ & + 4(1+2n_{\mathrm{B}})\eta(1-\eta)(|\alpha_n|^2 + |\beta_n|^2) \\ & + 12\,(1+2n_{\mathrm{B}})^2\eta^2|\alpha_n|^2|\beta_n|^2], \end{aligned} \quad (27)$$

$$\begin{aligned} Y = {} & (16\eta(1+2n_{\mathrm{B}}))^2[64(1-\eta)^2|\alpha_n|^2|\beta_n|^2 \\ & + 64(1+2n_{\mathrm{B}})^2\eta^2(|\alpha_n|^4 + |\beta_n|^4)|\alpha_n|^2|\beta_n|^2 \\ & + 128(1+2n_{\mathrm{B}})\eta(1-\eta)(|\alpha_n|^2 + |\beta_n|^2)|\alpha_n|^2|\beta_n|^2 \\ & + 128(1+2n_{\mathrm{B}})^2\eta^2|\alpha_n|^4|\beta_n|^4]. \end{aligned} \quad (28)$$

As a check, this expression reduces to Eq. (23) obtained in the previous section in the limit $\eta \to 1$ (no losses). Furthermore, $E_{\mathcal{N}}[n]$ vanishes when $\eta \to 0$, as expected, since in this limit none of the pairs created by the expansion get registered in the detectors. In between these limits, $E_{\mathcal{N}}[n]$ decreases monotonically when $\eta \to 0$. Unsurprisingly, losses and inefficiencies are sources of dissipation of quantum coherence or entanglement. Figure 7 shows $E_{\mathcal{N}}[n]$ for different values of η, showing that more efficient detectors (i.e., with smaller η) have more depletion of entanglement.

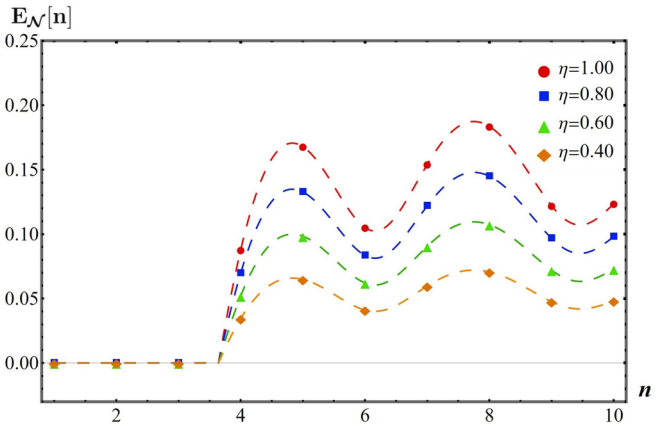

FIG. 7. Logarithmic negativity between phonons labeled by n and $-n$, for various values of the efficiency parameter $\eta = 1$ (*red circles*), $\eta = 0.80$ (*blue squares*), $\eta = 0.6$ (*green triangles*), and $\eta = 0.4$ (*orange diamonds*). For this plot, we took the parameters in Fig. 1, the environment temperature $T = 0.5$ nK, and the quantum pressure $\gamma = 0.5$.

D. Single-mode squeezed states and inputs

In view of the fragility of quantum entanglement to thermal noise and losses, it is of interest to envisage mechanisms to amplify these quantum correlations. Such a mechanism would assist in keeping alive the quantum signature of the pair-creation process in situations where the conditions of the experiment would otherwise render the final state completely classical.

We use a mechanism proposed in Refs. [39,40], consisting of replacing the initial vacuum, before the expansion of the BEC ring, by a *single-mode squeezed state*. Such a state is separable, in the sense that it does not contain entanglement between any mode with index n. However, it contains initial quanta which stimulate the production of additional entangled pairs. This stimulated creation strengthens the entanglement in the final state, making it more robust under deleterious effects. However, this mechanism does not create entanglement by itself: the final system entanglement would be zero if the BEC ring does not expand (since the initial excitations are unentangled), and in this sense the entanglement in the final state can all be attributed to the expansion. The initial squeezing acts as a "catalyzer" for the generation of entanglement.

From the point of view of quantum resource theory [50,51], single-mode squeezing (along with entanglement) is an available quantum resource, and the strengthening of entanglement during expansion can be regarded an interconversion of these resources. An alternative approach to augmenting entanglement production involves incorporating two-mode squeezing into the initial state. However, two-mode squeezing also introduces entanglement. Consequently, if entanglement is detected in the final state, it would not be feasible to attribute it solely to the expansion process. Note that here we do not

consider other nonclassical initial states, such as Fock states (which are difficult to create experimentally), since they lie outside the realm of Gaussian states that are our primary focus.

The limitation of our strategy to amplify or catalyze the production of entanglement is the difficulty of generating phonons in single-mode squeezed states in the laboratory. We postpone for future work the question of how a toroidal BEC experiment may realize a single-mode squeezed initial state, taking the point of view that the strategy presented in this section can be of interest as a concrete example for increasing the visibility of the quantum signatures of the pair-creation process.[4]

We proceed to consider an initial phonon state for the mode pair $(n, -n)$ corresponding to a single-mode squeezed state with thermal noise in it. This is a Gaussian state of the form (suppressing the mode index label)

$$\boldsymbol{\mu}_r^{(\mathrm{in})} = (0,0,0,0)^\top, \tag{29}$$

$$\boldsymbol{\sigma}_r^{\mathrm{in}} = (1+2n_{\mathrm{B}}) \begin{bmatrix} e^{2r} & 0 & 0 & 0 \\ 0 & e^{-2r} & 0 & 0 \\ 0 & 0 & 1 & 0 \\ 0 & 0 & 0 & 1 \end{bmatrix}. \tag{30}$$

In this state, the mode $-n$ is in a thermal state, while the mode n is in a thermal-squeezed state with squeezing intensity $r \in \mathbb{R}$. The modes are uncorrelated. In the limit $r \to 0$ this state reduces to the thermal state used in the previous section. We have chosen the squeezing in a particular "direction"—namely, we have squeezed the state in the $\hat{p}_n$ direction, and antisqueezed in $\hat{x}_n$ direction. The direction of the squeezing can be controlled by introducing a squeezing angle ϕ. The results of this section are independent of the choice of ϕ, so we will use $\phi = 0$ for simplicity in the presentation.

Following the strategy used in the previous section, we can compute the covariance matrix of the final state as $\boldsymbol{\sigma}_r^{(\mathrm{out})} = \mathbf{S} \cdot \boldsymbol{\sigma}_r^{(\mathrm{in})} \cdot \mathbf{S}^\top$, and compute from it the logarithmic negativity. Note that we also include losses parametrized by η in this calculation. We obtain

$$E_{\mathcal{N}}[n] = \max(0, -\log_2 \nu_{\mathrm{T},r,\eta}[n]) \tag{31}$$

where

$$\nu_{\mathrm{T},r,\eta}[n] = \frac{1}{4\sqrt{2}} \sqrt{X_r - \sqrt{Y_r}}, \tag{32}$$

$$\begin{aligned} X_r = {} & 16[2(1-\eta)^2 + 2(1+2n_{\mathrm{B}})^2\eta^2(|\alpha_n|^4 + |\beta_n|^4) \\ & + 4(1+2n_{\mathrm{B}})\eta(1-\eta)\cosh^2 r(|\alpha_n|^2 + |\beta_n|^2) \\ & + 4(1+2n_{\mathrm{B}})^2\eta^2[1+2\cosh(2r)]|\alpha_n|^2|\beta_n|^2], \end{aligned} \tag{33}$$

[4]The process of preparing a single-mode squeezed state may introduce supplementary noise into the initial state. If this noise exceeds a certain threshold, it could offset the advantages gained from squeezing. Consequently, when considering a mechanism for generating squeezing, it is important to evaluate the interplay between squeezing and the introduced noise. This paper provides the necessary tools to quantify this interplay.

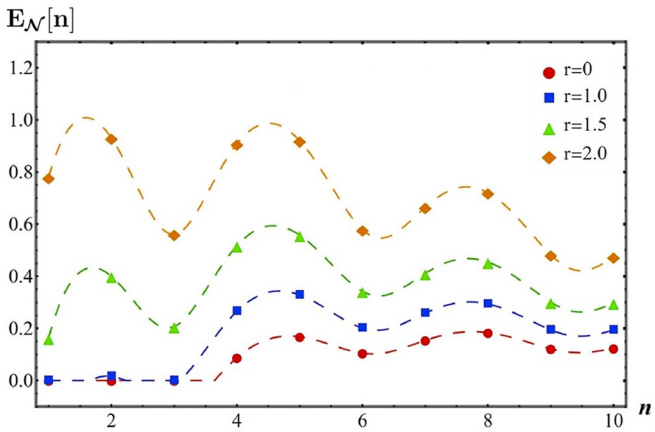

FIG. 8. Logarithmic negativity $E_{\mathcal{N}}[n]$ for pairs $(n, -n)$, vs the squeezing intensity r and ambient temperature $T = 0.5\,\mathrm{nK}$. Various values of initial squeezing r are shown. This plot corresponds to quantum pressure $\gamma = 0.5$ and $\eta = 1$, with the rest of the parameters being the same as in previous plots.

$$\begin{aligned} Y_r = {} & (16\eta(1+2n_{\mathrm{B}}))^2[16\sinh^4 r(1-\eta)^2(|\alpha_n|^4 + |\beta_n|^4) \\ & + 4(1-\eta)^2[3 + 12\cosh(2r) + \cosh(4r)]|\alpha_n|^2|\beta_n|^2 \\ & + 64(1+2n_{\mathrm{B}})^2\eta^2\cosh^2 r(|\alpha_n|^4 + |\beta_n|^4)|\alpha_n|^2|\beta_n|^2 \\ & + 128(1+2n_{\mathrm{B}})\eta(1-\eta)\cosh^4 r(|\alpha_n|^2 + |\beta_n|^2)|\alpha_n|^2|\beta_n|^2 \\ & + 128(1+2n_{\mathrm{B}})^2\eta^2\cosh^2 r\cosh(2r)|\alpha_n|^4|\beta_n|^4]. \end{aligned} \tag{34}$$

These expressions reduce to Eqs. (26) and (27) obtained in the last section in the limit $r \to 0$. The physical content in these expressions is shown in Fig. 8, which corresponds to a situation with no losses ($\eta = 1$). This plot shows the way initial squeezing amplifies the entanglement in the final state, and compensates for the deleterious effects of thermal noise. Figure 9 shows how the entanglement degrades due to

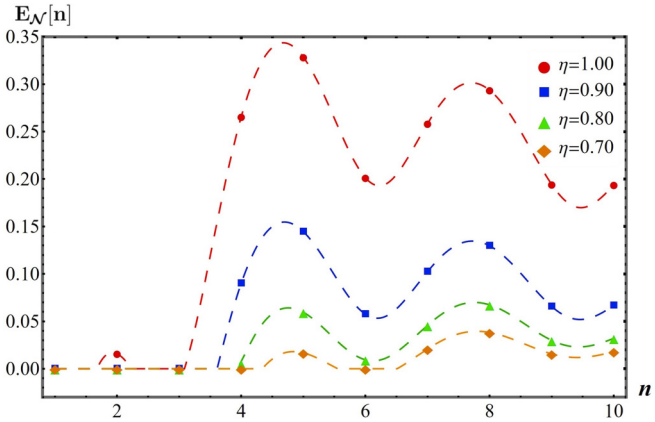

FIG. 9. Logarithmic negativity between phonons labeled by n and $-n$, for various values of the efficiency parameter $\eta = 1$ (*red*), $\eta = 0.80$ (*blue*), $\eta = 0.6$ (*green*), and $\eta = 0.8$ (*red*). For this plot, we took the parameters in Fig. 1, the environment temperature $T = 0.5\,\mathrm{nK}$, the quantum pressure $\gamma = 0.5$, and the single-mode squeezing parameter $r = 1.0$.

imperfect detectors even if we start with a thermal single-mode squeezed state of phonons.

To summarize, in this section, we have discussed that, in order to quantify entanglement, we need to construct the covariance matrix which is basically a collection of all possible correlations between phonon modes. The PPT criterion and logarithmic negativity then help us quantify the amount of entanglement in the phonon pairs for different choices of the initial quantum state, i.e., vacuum, thermal, and single-mode squeezed states. In the next section, we propose a protocol that can measure these mode correlations, thereby experimentally revealing the entanglement structure of phonons in an expanding toroidal BEC.

IV. PROTOCOL TO MEASURE ENTANGLEMENT

Observing entanglement in realistic situations is a challenging task. In this section, we discuss a possible strategy to achieve this goal adapted to the system we study in this paper. This proposal contains several idealized ingredients, which could give rise to challenges in realistic situations. It nevertheless provides a concrete set of ideas which can be useful as the starting point of a more refined protocol adapted to concrete experimental setups.

As discussed in Appendix B, there is a tradeoff in the use of logarithmic negativity compared to simpler entanglement witnesses, such as the Bell-like inequality $\Delta < 0$ [with Δ defined in Eq. (B18)]. While Δ involves only a few moments of the final state, it only indicates whether entanglement is present in the final state in certain circumstances. More precisely, the limitations of this inequality are two.

(i) It is not faithful, in the sense that $\Delta \geqslant 0$ does not rule out the existence of entanglement.

(ii) It is not a quantifier, because a stronger violation of the inequality does not necessarily imply more entanglement.

On the other hand, logarithmic negativity is a faithful quantifier for the simple systems we are interested in, namely Gaussian states and single-mode subsystems. The tradeoff is that its evaluation requires knowledge of the entire covariance matrix of the final state, which amounts to having full knowledge of the state.

To measure the elements of the covariance matrix of an inflationary toroidal BEC, we propose a generalization of the method due to Hellweg *et al.* [52], who measured the phase correlation function of a trapped BEC via a scheme that is analogous to the well-known stellar interferometry measurements of Hanbury-Brown and Twiss [53–55]. Hellweg *et al.* [52] accomplished this in two steps: first, by using Bragg diffraction to split the BEC into two identical copies (with a controllable phase difference between them); importantly, these two copies were shifted spatially relative to each other. The second step is to interfere the two separated condensates, measuring density correlations in the final system. The result of this final measurement reflects *phase* correlations of the original BEC.

In generalizing this scheme to the present case, it is not sufficient to merely extract phase correlations. Indeed, we also require density-density and phase-density correlations, as a function of angle, i.e., we need the correlation functions

$$C_{\hat{n}_1\hat{n}_1}(\alpha) := \langle\{\hat{n}_1(\alpha), \hat{n}_1(0)\}\rangle, \tag{35}$$

$$C_{\hat{\phi}_1\hat{\phi}_1}(\alpha) := \langle\{\hat{\phi}_1(\alpha), \hat{\phi}_1(0)\}\rangle, \tag{36}$$

$$C_{\hat{n}_1\hat{\phi}_1}(\alpha) := \langle\{\hat{n}_1(\alpha), \hat{\phi}_1(0)\}\rangle, \tag{37}$$

where α is the separation angle. From these functions, we can obtain the correlations between modes $(n, -n)$ by a simple Fourier transform, as we discuss below. Since a Gaussian state is completely determined by the set of quadratic correlation functions, it makes sense that these three functions are sufficient to reproduce the full covariance matrix. Mathematically, the connection comes from Eqs. (3) that relate density and phase fluctuations to the mode operators $\hat{a}_n^\dagger$ and $\hat{a}_n$, and via Eq. (14) that connects the mode operators to $\hat{x}_n$ and $\hat{p}_n$.

To see how these correlation functions could be measured, we now describe a natural generalization of the Hellweg *et al.* [52] steps to the present case of an expanding toroidal BEC, as illustrated in Fig. 10. The first step assumes it is possible to use Bragg diffraction to split the original toroidal BEC into two identical copies, with an induced phase δ between them (that is experimentally controllable). We also assume the resulting clouds can be rotated an angle α relative to each other, after which they are allowed to evolve freely for some time. Finally, the clouds are interfered, with density correlations being measured in the final system. The preceding steps can be encapsulated in the following expression for the final condensate field operator as a function of angle θ:

$$\hat{\Phi}(\theta) = \tfrac{1}{2}\Big[\sqrt{n_0 + \hat{n}_1(\theta - \alpha/2)}\,e^{i(\phi_0 + \hat{\phi}_1(\theta-\alpha/2))} + e^{i\delta}\sqrt{n_0 + \hat{n}_1(\theta + \alpha/2)}\,e^{i(\phi_0 + \hat{\phi}_1(\theta+\alpha/2))}\Big], \tag{38}$$

which also depends on the controllable angular displacement α and controllable phase difference δ. Here, we have made use of the Madelung representation $\hat{\Phi}(\theta) = \sqrt{\hat{n}}\,e^{i\hat{\phi}}$, with $\hat{n} = n_0 + \hat{n}_1(\theta)$ and $\hat{\phi} = \phi_0 + \hat{\phi}_1(\theta)$, as described in Eqs. (1) and (2). Equation (38) is precisely an angular version of Eq. (5) of Hellweg *et al.* [52].

Now we show that a measurement of the condensate density two-point correlation function at coincident points, $\langle\hat{N}(\theta)\hat{N}(\theta)\rangle_{\alpha,\delta}$, where $\hat{N}(\theta) = \hat{\Phi}^\dagger(\theta)\hat{\Phi}(\theta)$, contains the correlations we are looking for, as we describe now—the labels α and δ remind us about the rotation angle α and induced Bragg phase δ chosen in the procedure. Let us focus on an arbitrary point of the final cloud, which, without loss of generality, we can choose as $\theta = 0$. Then, the symmetric correlator $\langle\{\hat{N}(0), \hat{N}(0)\}\rangle_{\alpha,\delta}$ obtained is related to phase $\hat{\phi}_1(\theta)$ and density $\hat{n}_1(\theta)$ two-point correlators by

$$\langle\{\hat{N}(0), \hat{N}(0)\}\rangle_{\alpha,\delta} = \frac{1}{2}n_0^2(1+\cos\delta)^2 + \frac{1}{16}\Big[\tilde{C}_{\hat{n}_1\hat{n}_1}(\alpha)\,(1+\cos\delta)^2 + \tilde{C}_{\hat{\phi}_1\hat{\phi}_1}(\alpha)\,4n_0^2\,\sin^2\delta\Big] \tag{39}$$

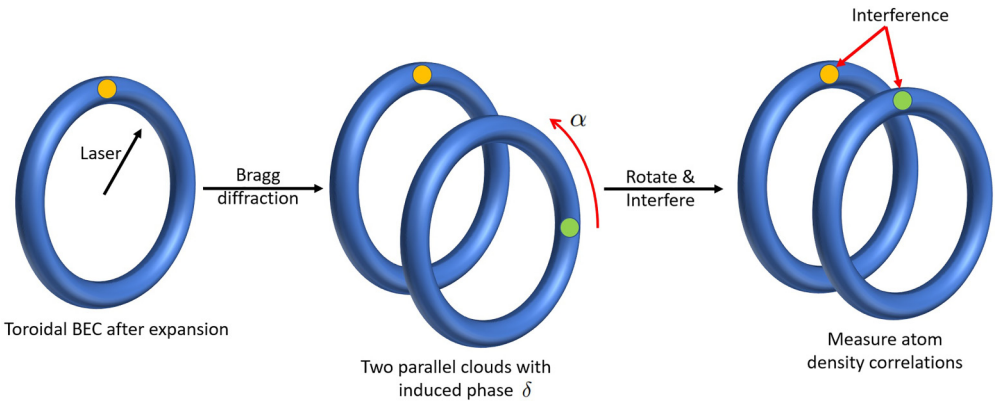

FIG. 10. A schematic figure showing the protocol to measure mode entanglement in the BEC. The first stage (first panel) is where the expanded BEC is Bragg diffracted using a laser, which then splits into two parallel clouds with an induced phase difference of δ. Then, in the second stage (second panel), one of the rings is rotated by some angle α which brings the two points (shown in green and orange colors) in front of each other. In the third stage (third panel), the two clouds are made to interfere with each other and the atom density correlations are obtained. This setup would allow the extraction of all types of correlations between phase and density fluctuations, and thus the covariance matrix can be built.

where we have defined

$$\tilde{C}_{\hat{n}_1\hat{n}_1}(\alpha) \equiv -2[C_{\hat{n}_1\hat{n}_1}(\alpha) - C_{\hat{n}_1\hat{n}_1}(0)], \tag{40}$$

$$\tilde{C}_{\hat{\phi}_1\hat{\phi}_1}(\alpha) \equiv -2[C_{\hat{\phi}_1\hat{\phi}_1}(\alpha) - C_{\hat{\phi}_1\hat{\phi}_1}(0)]. \tag{41}$$

Therefore, by measuring $\langle\{\hat{N}(0), \hat{N}(0)\}\rangle_{\alpha,\delta}$ for two different induced phases, say δ_1 and δ_2, and fixing the relative rotation angle α, the above linear equation can be solved for $\tilde{C}_{\hat{n}_1\hat{n}_1}(\alpha)$ and $\tilde{C}_{\hat{\phi}_1\hat{\phi}_1}(\alpha)$. From these correlations it is simple to obtain the correlations functions we are actually interested in—$C_{\hat{n}_1\hat{n}_1}(\alpha)$ and $C_{\hat{\phi}_1\hat{\phi}_1}(\alpha)$—by noticing that

$$\frac{1}{4\pi}\int_0^{2\pi} d\alpha\, C_{\hat{n}_1\hat{n}_1}(\alpha) = 0. \tag{42}$$

This is because $C_{\hat{n}_1\hat{n}_1}(\alpha)$ does not include the zero mode $n = 0$ in its Fourier series, since this homogeneous mode has been absorbed in the background condensate n_0. Thus, integrating (40) over all possible rotation angles α, and making use of (42), produces $2\,C_{\hat{n}_1\hat{n}_1}(0)$. The same argument applies to $C_{\hat{\phi}_1\hat{\phi}_1}(\alpha)$. Thus, the elementary density-density and phase-phase correlations can be extracted as follows:

$$C_{\hat{n}_1\hat{n}_1}(\alpha) = -\frac{1}{2}\tilde{C}_{\hat{n}_1\hat{n}_1}(\alpha) + \frac{1}{4\pi}\int_0^{2\pi} d\alpha\, \tilde{C}_{\hat{n}_1\hat{n}_1}(\alpha), \tag{43}$$

$$C_{\hat{\phi}_1\hat{\phi}_1}(\alpha) = -\frac{1}{2}\tilde{C}_{\hat{\phi}_1\hat{\phi}_1}(\alpha) + \frac{1}{4\pi}\int_0^{2\pi} d\alpha\, \tilde{C}_{\hat{\phi}_1\hat{\phi}_1}(\alpha). \tag{44}$$

[Note that $C_{\hat{n}_1\hat{n}_1}(\alpha)$ can be directly measured in the original toroidal BEC, without the interferometry steps; so, as a check, one could compare such a direct observation with the result obtained from (43).]

It remains to determine the mixed density-phase correlations $C_{\hat{n}_1\hat{\phi}_1}(\alpha)$. Since $\hat{\phi}_1$ and $\hat{n}_1$ are related by $\hat{n}_1 = -\frac{\hbar\mathcal{V}}{U}\frac{d}{dt}\hat{\phi}_1$, the missing correlation function can be obtained by taking time derivative of $C_{\hat{\phi}_1\hat{\phi}_1}(\alpha)(t)$. This requires a repetition of the above steps for different times after expansion $t > t_f$, in discrete time intervals. That is, after expansion, Bragg diffraction, rotation, and interference, we require a measurement of the correlations at time $t = t_f$ and a measurement of the same for an identically prepared condensate at $t = t_f + \Delta t$. The time interval Δt should be small compared to any other timescales in the problem, such as the frequency associated with the smallest mode $\omega^{\rm f}_{n=1} \equiv c/R(t_{\rm f})$, or the timescale associated with the damping of density fluctuations, as was seen in Ref. [27]. This procedure yields the time evolution data for the phase-phase correlations, from which we can obtain the mixed correlation function:

$$C_{\hat{n}_1\hat{\phi}_1}(\alpha) \equiv \langle\{\hat{n}_1(\alpha,t), \hat{\phi}_1(0,t)\}\rangle = -\frac{1}{2}\frac{\hbar\mathcal{V}_f}{U}\frac{d}{dt}C_{\hat{\phi}_1\hat{\phi}_1}(\alpha,t),$$

where we have defined $\mathcal{V}_f \equiv \mathcal{V}(t_f)$, and have made use of Eq. (A7) that relates the density operator to the time derivative of the phase operator and approximated the quantum pressure operator $\hat{\mathcal{D}}_\theta \simeq 1$.

Once the two-point correlations in real space are known, we can obtain the covariance matrix of the final state as follows. First, from $C_{\hat{n}_1\hat{n}_1}(\alpha)$, $C_{\hat{\phi}_1\hat{\phi}_1}(\alpha)$, and $C_{\hat{n}_1\hat{\phi}_1}(\alpha)$ we can obtain the symmetrized second moments of the creation and annihilation operators as follows:

$$\begin{aligned}\left\langle\left\{\hat{a}_n^{(\rm out)}, \hat{a}_{-n}^{(\rm out)}\right\}\right\rangle &= p_f\int_0^{2\pi} d\alpha\, e^{-in\alpha}\big[(\chi_n^*)^2 C_{\hat{n}_1\hat{n}_1}(\alpha) \\ &\quad + \mathcal{V}_f^2(\eta_n^*)^2 C_{\hat{\phi}_1\hat{\phi}_1}(\alpha) - 2\mathcal{V}_f\chi_n^*\eta_n^* C_{\hat{n}_1\hat{\phi}_1}(\alpha)\big], \\ \left\langle\left\{\hat{a}_n^{(\rm out)}, \hat{a}_n^{(\rm out)\,\dagger}\right\}\right\rangle &= -p_f\int_0^{2\pi} d\alpha\, e^{-in\alpha} \\ &\quad \times\big[|\chi_n|^2 C_{\hat{n}_1\hat{n}_1}(\alpha) + \mathcal{V}_f^2|\eta_n|^2 C_{\hat{\phi}_1\hat{\phi}_1}(\alpha)\big],\end{aligned} \tag{45}$$

where we have defined the proportionality constant to be $p_f = -a_f^{1+2\gamma}\frac{U}{\hbar\mathcal{V}_f}$, and we have suppressed the term "out" in the mode functions for phase $\chi_n^{(\rm out)} = (2\omega_n^f a_f^{1+\gamma})^{-1/2}e^{-i\omega_n^f(t-t_f)}$, and density $\eta_n^{(\rm out)} = -i\frac{\hbar}{U}\sqrt{\frac{\omega_n^f}{2a_f^{1+\gamma}}}e^{-i\omega_n^f(t-t_f)}$. The rest of the independent second moments, $\langle\{\hat{a}_n^{(\rm out)}, \hat{a}_n^{(\rm out)}\}\rangle$ and $\langle\{\hat{a}_n^{(\rm out)}, \hat{a}_{-n}^{(\rm out)\,\dagger}\}\rangle$, are zero.

With these moments we have full information of the covariance matrix of the final state in the creation and annihilation variables

$$\boldsymbol{\sigma}^{\rm out}_{(\mathbf{A},n)} = \langle\{\hat{\mathbf{A}}^{\rm (out)}_n, \hat{\mathbf{A}}^{\rm (out)}_n\}\rangle, \tag{46}$$

out of which we obtain the covariance matrix we are looking for as $\boldsymbol{\sigma}^{\rm out}_{(n)} = \mathbf{B}\cdot\boldsymbol{\sigma}^{\rm out}_{(\mathbf{A},n)}\cdot\mathbf{B}^{-1}$, where the change-of-basis matrix $\mathbf{B}$ is given in Eq. (B5). Then, following the procedure outlined in Sec. III, we can quantify the quantum correlations in this system via the logarithmic negativity $E_{\mathcal{N}}[n]$, that determines the amount of entanglement in the phonon mode pairs $(n, -n)$ in the expanding toroidal BEC.

The preceding analysis also gives us a hint as to what types of quantum correlations in the toroidal BEC lead to more entanglement, i.e., larger logarithmic negativity. Following the discussions in Sec. III and Appendix B, we note that in the present two-mode case the covariance matrix is a 4×4 matrix, so that there are two symplectic eigenvalues of the partially transposed covariance matrix. Since only the minimum of these two (which we call $\nu_{\rm min}$) can be less than unity (and contribute to the logarithmic negativity), it is sufficient to focus on $\nu_{\rm min}$, which can be written in terms of the mode space correlators given in Eq. (45):

$$\nu_{\rm min} = \langle\{\hat{a}^{\rm (out)}_n, \hat{a}^{\rm (out)\,\dagger}_n\}\rangle - |\langle\{\hat{a}^{\rm (out)}_n, \hat{a}^{\rm (out)}_{-n}\}\rangle|. \tag{47}$$

Since the logarithmic negativity $E_{\mathcal{N}}[n]$ is related to the logarithm of $\nu_{\rm min}$, in order to maximize entanglement, we need this eigenvalue to approach zero. Using Eq. (45), we can express this condition in terms of real space correlators:

$$\nu_{\rm min} = -A_+ - \sqrt{A_-^2 + B^2}, \tag{48}$$

where the functions $A_\pm$ and B are defined as follows:

$$A_\pm = |\chi_n|^2 C_{\hat{n}_1\hat{n}_1}(n) \pm |\eta_n|^2 C_{\hat{\phi}_1\hat{\phi}_1}(n), \tag{49}$$

$$B = 2|\chi_n||\eta_n| C_{\hat{n}_1\hat{\phi}_1}(n), \tag{50}$$

where we define the Fourier transforms of the real-space correlators:

$$C_{\hat{n}_1\hat{n}_1}(n) = p_f \int_0^{2\pi} d\alpha\; e^{-in\alpha} C_{\hat{n}_1\hat{n}_1}(\alpha), \tag{51}$$

$$C_{\hat{\phi}_1\hat{\phi}_1}(n) = p_f \mathcal{V}_f^2 \int_0^{2\pi} d\alpha\; e^{-in\alpha} C_{\hat{\phi}_1\hat{\phi}_1}(\alpha), \tag{52}$$

$$C_{\hat{n}_1\hat{\phi}_1}(n) = p_f \mathcal{V}_f \int_0^{2\pi} d\alpha\; e^{-in\alpha} C_{\hat{n}_1\hat{\phi}_1}(\alpha). \tag{53}$$

To maximize entanglement, we need $\nu_{\rm min}$ to be small. Setting Eq. (48) to vanish, putting the square root on one side, and squaring both sides leads to

$$C_{\hat{n}_1\hat{n}_1}(n) C_{\hat{\phi}_1\hat{\phi}_1}(n) = [C_{\hat{n}_1\hat{\phi}_1}(n)]^2, \tag{54}$$

a condition on the correlation functions, as a function of mode index, that maximizes $E_{\mathcal{N}}[n]$.

V. CONCLUDING REMARKS

This paper provides a quantitative analysis of the generation of quantum entanglement in the process of pair creation in a thin toroidal BEC with a time dependent radius. This system constitutes an analog simulator for the behavior of quantum fields propagating in an expanding universe, and in particular during inflation. Such expanding BEC rings have been experimentally produced [27,28], where the redshift of density perturbations induced by the expansion and an analog of the process of reheating have been observed. The phonon pair-production phenomenon in this system, triggered by the expansion, was then studied theoretically in Ref. [30], using a model based on the Bogoliubov–de Gennes (BdG) Hamiltonian, which in the thin-ring limit produces equations of motion for azimuthal phonons that are analogous to the Mukhanov-Sasaki equation that describes scalar curvature perturbations in cosmology.

The generation of entanglement constitutes the quantum signature of the pair-creation process and its observation would be a smoking gun for the quantum origin of the observed density perturbations. The goal of this paper is to quantify such entanglement and to propose ways of measuring it. Special attention has been paid in this paper to include the effects of thermal noise, losses, and detector inefficiencies.

Our analysis can be applied to any expansion history of the thin ring, as long as the ring is not expanding in the initial and final regions. Having early- and late-time regions where the radius of the ring is time independent permits one to talk about particle creation, which in turn provides a way to talk about entanglement production. Note that in the real inflationary universe such in and out regions are not available, since the universe keeps expanding after inflation ends (and what happened before inflation is not yet understood); this implies that there is no unambiguous way to define particle creation and, consequently, the quantification of entanglement also becomes ambiguous [21]—except if one restricts attention to Fourier modes whose wavelengths are much shorter than the Hubble radius. In this sense, being able to engineer nonexpanding in and out regions is advantageous in the study of entanglement generation.

Techniques based on Gaussian states for continuous variable quantum systems are a powerful and efficient tool to quantify entanglement in this scenario. Our analysis has shown that, as one could intuitively expect, quantum entanglement is fragile to noise and losses. When losses can be approximated by a Gaussian channel, we have quantified the region in the parameter space where thermal noise and losses completely decohere the phonon pairs that would be otherwise entangled. Under such circumstances, all quantum signatures of the pair-creation process are gone, and one is left with the amplification of thermal noise by the expanding ring, a process that can be entirely accounted for in classical terms. Our analysis, therefore, helps to delineate the boundary where one could hope to observe genuine quantum effects.

We have further explored and introduced ideas, adapted from Refs. [39,40], to amplify the generation of entanglement, based on seeding the process with single-mode squeezed states, in order to compensate for the deleterious effects aforementioned, and to maintain the genuine quantum features generated by the expansion present in the final state. In addition, we have sketched a protocol (inspired by the experiments of Hellweg *et al.* [52]) to measure entanglement in the inflationary toroidal BEC. Although our protocol may require a prohibitively large amount of practical resources, it constitutes

a concrete example of what would be needed to fully reconstruct the final phonon state and to quantify entanglement.

We conclude this section by suggesting some directions for future work. We note that, although we have focused on an expanding BEC ring, our idea applies to other scenarios for simulating pair creation in expanding (or contracting) backgrounds, such as the two-dimensional quantum field simulator considered in Refs. [56,57].

Future studies could look into constructing protocols to detect entanglement in quantum states that have non-Gaussianity present in them. It would also be interesting to compare the procedure and results of this protocol with the experiments of Chen *et al.* [58], that explore how to witness entanglement inside a BEC using the Peres-Horodecki criterion.

In this paper, we studied how initial squeezing of one mode can amplify entanglement [39,40]; extensions of this analysis can include the case where modes n and $-n$ are individually squeezed, which may provide even more amplification of entanglement in the final state. Additionally, future work may investigate how such squeezing of the initial states may be accomplished in a realistic toroidal BEC experiment.

ACKNOWLEDGMENTS

The authors are grateful to Anthony Brady, Lior Cohen, Adrià Delhom, Stav Haldar, and Marlan Scully for useful comments and discussions. I.A. and D.K. are especially thankful to Anthony Brady; some of the tools used in this paper were developed in collaboration with him, and applied to analog Hawking radiation in optical systems. A.B. acknowledges financial support from the Department of Physics and Astronomy at LSU. A.B. and D.E.S. acknowledge financial support from NSF Grant No. PHY-2208036. I.A. and D.K. acknowledge financial support from NSF Grant No. PHY-2110273, and from the Hearne Institute for Theoretical Physics. J.W. acknowledges financial support from NSF Grant No. DMR-2238895. I.A. is also supported by the RCS program of Louisiana Board of Regents through Grant No. LEQSF(2023-25)-RD-A-04, and in part by Perimeter Institute for Theoretical Physics. Research at Perimeter Institute is supported by the Government of Canada through the Department of Innovation, Science, and Economic Development, and by the Province of Ontario through the Ministry of Colleges and Universities. J.W. performed part of this work at the Aspen Center for Physics, which is supported by NSF Grant No. PHY-2210452.

APPENDIX A: BEC IN AN EXPANDING TOROIDAL TRAP

In this Appendix, we fill in details, omitted from the main text, that connect the BdG formalism for an expanding toroidal BEC to the Mukhanov-Sasaki equation for inflationary perturbations [Eq. (4) of the main text]. We start from the following Hamiltonian for bosons in a position and time dependent toroidal potential $V(\boldsymbol{r},t)$, with $\hat{\Phi}(\boldsymbol{r},t)$ the boson field operator

$$\hat{H}=\int d^3r\left[\hat{\Phi}^\dagger(\boldsymbol{r},t)\hat{h}(\boldsymbol{r},t)\hat{\Phi}(\boldsymbol{r},t)+\frac{1}{2}U|\hat{\Phi}(\boldsymbol{r},t)|^4\right], \tag{A1}$$

where $\hat{h}(\boldsymbol{r},t)\equiv[-\frac{\hbar^2}{2M}\nabla^2+V(\boldsymbol{r},t)-\mu]$, μ is the chemical potential, $U=\frac{4\pi a_s\hbar^2}{M}$ is the interaction parameter, a_s is the scattering length, $\hbar$ is Planck's constant, and M is the mass of the bosonic atoms. The toroidal atom trap can be modeled using a "flat-bottomed" potential which, in cylindrical coordinates (ρ,θ,z), is

$$V(\boldsymbol{r},t)=\lambda|\rho-R(t)|^{n_t}+\tfrac{1}{2}M\omega_z^2z^2, \tag{A2}$$

where λ and ω_z characterize the confinement in the radial and vertical directions, respectively, and $R(t)$ is the external radius of the toroid. In the experiment of Ref. [27], the parameter $n_t=4$. The condensate field operator obeys the commutation relation $[\hat{\Phi}(\boldsymbol{r},t),\hat{\Phi}^\dagger(\boldsymbol{r}',t)]=\delta^{(3)}(\boldsymbol{r}-\boldsymbol{r}')$. Plugging the Hamiltonian into the Heisenberg equation of motion $-i\hbar\frac{d\hat{A}}{dt}=-i\hbar\frac{\partial\hat{A}}{\partial t}+[\hat{H},\hat{A}]$, and making use of the commutation relations for $\hat{\Phi}(\boldsymbol{r},t)$, leads to the operator equations of motion:

$$i\hbar\partial_t\hat{\Phi}(\boldsymbol{r},t)=\hat{h}(\boldsymbol{r},t)\hat{\Phi}(\boldsymbol{r},t)+U\hat{\Phi}^\dagger(\boldsymbol{r},t)\hat{\Phi}(\boldsymbol{r},t)\hat{\Phi}(\boldsymbol{r},t). \tag{A3}$$

For a study of perturbations, we make use of the Bogoliubov approximation that expresses the condensate field in terms of a coherent background $\hat{\Phi}_0$ and perturbations $\delta\hat{\varphi}$:

$$\hat{\Phi}=\Phi_0(1+\delta\hat{\varphi}). \tag{A4}$$

The strategy is to plug Eq. (A4) into Eq. (A3) and expand order by order in $\delta\hat{\varphi}$, finding approximate equations of motion at each order. The zeroth order in $\delta\hat{\varphi}$ simply yields the Gross-Pitaevskii equation for $\Phi_0(\mathbf{r},t)$, which has the same form as Eq. (A3) but with the replacement $\hat{\Phi}\to\Phi_0$. Importantly, we will not assume $\Phi_0(\mathbf{r},t)$ to be static, but rather exhibit time dependent dynamics due to the expanding toroidal trap.

Our main interest is the equation of motion to first order in $\delta\hat{\varphi}$, essentially the BdG equations for this system. In doing this, we find it convenient to switch to the Madelung representation for the fluctuations, by expressing the condensate field in terms of density $\hat{n}(\boldsymbol{r},t)$ and phase $\hat{\phi}(\boldsymbol{r},t)$ field operators: $\hat{\Phi}(\boldsymbol{r},t)=\sqrt{\hat{n}(\boldsymbol{r},t)}e^{i\hat{\phi}(\boldsymbol{r},t)}$. Introducing linear perturbations for the phase $\hat{\phi}=\phi_0+\hat{\phi}_1$ and the density $\hat{n}=n_0+\hat{n}_1$, to first order we get an expression for the condensate perturbation $\delta\hat{\varphi}$ in terms of perturbations in density $\hat{n}_1(\boldsymbol{r},t)$ and phase $\hat{\phi}_1(\boldsymbol{r},t)$:

$$\delta\hat{\varphi}(\boldsymbol{r},t)=\frac{\hat{n}_1(\boldsymbol{r},t)}{2n_0(\boldsymbol{r},t)}+i\hat{\phi}_1(\boldsymbol{r},t), \tag{A5}$$

where $\phi_0(\boldsymbol{r},t)$ and $n_0(\boldsymbol{r},t)\equiv|\Phi_0(\boldsymbol{r},t)|^2$ denote the background phase and density, respectively, and the perturbations satisfy $[\hat{n}_1(\boldsymbol{r},t),\hat{\phi}_1(\boldsymbol{r}',t)]=i\delta^{(3)}(\boldsymbol{r}-\boldsymbol{r}')$.

In terms of these perturbations, the linear-order equation of motion following from Eq. (A3) can be written compactly as

$$i\hbar\partial_t\big(\delta\hat{\varphi}\big)=-\frac{\hbar^2}{2m}\Big(\frac{2\nabla\Phi_0\cdot\nabla}{\Phi_0}+\nabla^2\Big)\delta\hat{\varphi}+U\hat{n}_1. \tag{A6}$$

This formula includes both representations of the linear perturbations, and below we seek formulas only including $\hat{n}_1$ and $\hat{\phi}_1$. When we do this we will also make some simplifying approximations due to the geometry of the toroid. The first approximation is to neglect the ρ and z dependencies of the phase and density perturbations, thereby replacing $\hat{\phi}_1(\boldsymbol{r},t)\to$

$\hat{\phi}_1(\theta,t)$ and $\hat{n}_1(\boldsymbol{r},t) \to \mathcal{V}^{-1}\hat{n}_1(\theta,t)$, where $\mathcal{V} = R\mathcal{A}$ is a volume scale with $\mathcal{A}$ the cross-sectional area of the toroid (so that $2\pi\mathcal{V}$ is the toroid volume).

The preceding steps hold in the thin-ring limit, where the toroidal radius $R(t)$ is much larger than the typical length scales characterizing the ring cross-sectional area. This implies that an initial angle-dependent perturbation around the ring will not excite density variations in the ρ and z directions. Next, we assume that, since the toroid is symmetric with respect to angular variations, we can assume that the background phase ϕ_0 and density n_0 are independent of the angle θ. Finally, we assume that the superfluid velocity equals the ring velocity $\boldsymbol{v} = \frac{\hbar}{M}\nabla\phi_0 = \dot{R}\hat{\rho}$ (here $\dot{R} \equiv \frac{dR}{dt}$), implying that the gradients of perturbations are orthogonal to the condensate velocity, i.e., $\boldsymbol{v}\cdot\nabla\hat{\phi}_1 = 0$ and $\boldsymbol{v}\cdot\nabla\hat{n}_1 = 0$. However, note that the divergence of condensate velocity is not zero: $\nabla\cdot\boldsymbol{v} = \frac{\hbar}{M}\nabla^2\phi_0 \approx \frac{\dot{R}}{R}$.

Substituting the relation (A5) into (A6), using the above approximations, and taking the real and imaginary parts of the resulting expression, we finally obtain

$$-\frac{\hbar}{U}\partial_t\hat{\phi}_1 = \hat{\mathcal{D}}_\theta\hat{n}_1, \tag{A7}$$

$$\partial_t\hat{n}_1 = -\frac{\dot{R}}{R}n_1 - \frac{\hbar n_0}{MR^2}\partial_\theta^2\phi_1, \tag{A8}$$

essentially the Euler and continuity equations for the phase and density perturbations in the thin-ring limit. Here, $\hat{\mathcal{D}}_\theta \equiv 1 - \frac{\hbar^2}{2MU}\left(\frac{\partial_\theta^2}{2n_0R^2} - \frac{\nabla^2 n_0}{2n_0^2} + \frac{(\nabla n_0)^2}{2n_0^3}\right)$ accounts for quantum pressure contributions to the equations of motion.

The next step is to plug in the operator expansion formulas Eqs. (3), which leads to

$$-\frac{\hbar}{U}\dot{\chi}_n = D_n\eta_n, \tag{A9}$$

$$\dot{\eta}_n = -\frac{\dot{R}}{R}\eta_n + \frac{\hbar n_0}{MR^2}n^2\chi_n, \tag{A10}$$

where now

$$D_n \equiv 1 + \frac{\hbar^2}{4MUn_0}\left(\frac{n^2}{R^2} + \frac{\nabla^2 n_0}{n_0} - \frac{(\nabla n_0)^2}{n_0^2}\right), \tag{A11}$$

where we emphasize that, generally, n_0 depends on ρ, z, and t. Upon eliminating η_n in favor of χ_n, we finally arrive at

$$\ddot{\chi}_n + (1+\gamma_n)\frac{\dot{R}}{R}\dot{\chi}_n + \alpha_n\frac{n^2c^2}{R^2}\chi_n = 0, \tag{A12}$$

where we have defined the speed of sound $c = \sqrt{\frac{Un_0}{M}}$ (which also generally depends on ρ, z, and t since it is a function of n_0) and the quantum pressure parameters

$$\gamma_n = -\frac{R\dot{D}_n}{\dot{R}D_n}, \tag{A13}$$

$$\alpha_n = D_n. \tag{A14}$$

In general, γ_n and α_n are dependent on the local atom density in the expanding toroidal trap (via n_0), as well as the time dependent ring radius R and the mode index n. These parameters will therefore be sensitive to the precise details of the experimental setup (such as the shape of the trapping potential). Nonetheless, following Ref. [30] we can make estimates based on the experiments of Ref. [27].

In making such estimates, we neglect the first term in parentheses on the right side of Eq. (A11), since it is $\propto R^{-2}$, while the latter terms are $\propto 1/w^2$, with w the condensate width across the toroid. Since we expect $w \ll R$, if the mode index n is not too large then neglecting this term is valid. Strictly, w is the width of the background condensate, and if we assume a Gaussian spatial profile for the condensate $n_0(\rho,z) = e^{-(\rho^2+z^2)/(2w)^2}$, then we get

$$D_n \simeq 1 - \frac{3}{8}\frac{\hbar^2}{c^2M^2w^2} = 1 - \frac{3}{4}\frac{\xi^2}{w^2} \tag{A15}$$

where c is now a constant, defined by approximating $n_0(\rho,z)$ by its value at $\rho \to 0$ and $z \to 0$ (the central density in the toroid). To get Eq. (A15), we made a similar approximation to the derivative terms of Eq. (A11), evaluating the derivatives before taking the limits $\rho \to 0$ and $z \to 0$. In the final equality of Eq. (A15), we expressed the result in terms of the coherence length $\xi = \frac{\hbar}{\sqrt{2}Mc}$.

If we assume $\xi \ll w$, which indeed holds for the experiments of Ref. [27], then we expect $D_n \simeq 1$. It is thus tempting (and arguably reasonable) to take $\alpha_n \simeq 1$ and $\gamma_n \simeq 0$ in Eq. (A12). As discussed in Ref. [30] (where the estimate $\gamma_n \approx 0.1$ is also found), this is valid for α_n, since a small deviation of α from unity can be absorbed into the speed of sound parameter c. Taking $\gamma_n \to 0$, however, qualitatively changes the behavior of Eq. (A12), since in that limit it can be written as (reintroducing time arguments which were previously suppressed)

$$\frac{1}{R(t)}\frac{d}{dt}[R(t)\dot{\chi}_n(t)] + \frac{n^2c^2}{R(t)^2}\chi_n(t) = 0, \tag{A16}$$

that is solved by

$$\chi_n(t) = \chi_n\exp\left[\pm in\int_0^t dt'\,\frac{c}{R(t')}\right], \tag{A17}$$

a solution that preserves the mode amplitude as a function of time during expansion. This means that, within our analysis, a toroidal BEC expanded according to Eq. (7) with $\gamma_n = 0$ will have zero particle production, i.e., $|\beta_n|^2 = 0$. By contrast, at nonzero $\gamma_n = \gamma$ the solution changes qualitatively, being given [for the case of $R(t) = R_0e^{t/\tau}$] by

$$\chi_n(t) = e^{-\frac{t}{2\tau}(1+\gamma)}[A_nJ_{\frac{1+\gamma}{2}}(z) + B_nJ_{-\frac{1+\gamma}{2}}(z)], \tag{A18}$$

with $z = \frac{nc\tau}{R(t)}$ and $J_n(z)$ the modified Bessel function. This tells us that, while the parameter γ is small, nonzero γ is crucial for the phenomenon of particle creation. Using a Thomas-Fermi-type approximation, along with parameters from Ref. [27], in Ref. [30] the estimate $\gamma \approx 10^{-1}$ was found. Since γ is small, but nonzero, in the main text we regard it as an experimentally determined parameter with $0 < \gamma < 1$.

APPENDIX B: GAUSSIAN STATES AND LINEAR EVOLUTION: A SHORT REVIEW

For self-consistency, in this Appendix we provide a summary of some elements of Gaussian states for continuous variable quantum systems and their evolution under quadratic

Hamiltonians. See Ref. [46] for proofs omitted here. Note that we choose units in which $\hbar = 1$ in this Appendix.

1. Evolution of linear systems with N degrees of freedom

Consider a dynamical system containing N classical degrees of freedom. Quantum mechanically the system is described by N pairs of canonically conjugate operators $\hat{x}_I$ and $\hat{p}_I$, with $I = 1, \cdots, N$. Let us define a vector $\hat{\mathbf{r}}$ made of all canonical pairs:

$$\hat{\mathbf{r}} = (\hat{x}_1, \hat{p}_1, \cdots, \hat{x}_N, \hat{p}_N)^\top. \tag{B1}$$

In the following, we will assume that $\hat{x}_I$ and $\hat{p}_I$ have been rescaled using the dimensionful constants of the problem under consideration to have dimensions of action, as commonly done when working with harmonic oscillators. Let $\hat{\mathbf{r}}^i$ be the ith component of $\hat{\mathbf{r}}$, where low case indices $i, j, \cdots$ run from 1 to $2N$ (capital letter indices $I, J, \cdots$, instead, run from 1 to N). Then, the canonical commutation relation can be succinctly written as

$$[\hat{\mathbf{r}}^i, \hat{\mathbf{r}}^j] = i\,\mathbf{\Omega}^{ij}, \quad \mathbf{\Omega} \equiv \bigoplus_N \begin{pmatrix} 0 & 1 \\ -1 & 0 \end{pmatrix}, \tag{B2}$$

where the antisymmetric matrix $\mathbf{\Omega}$ is the (inverse of the) symplectic form of the classical phase space.

We are interested in processes where there exist asymptotic regions in the past and future, where one can define preferred canonical operators $\hat{\mathbf{r}}_{(\text{in})}$ and $\hat{\mathbf{r}}_{(\text{out})}$, and an interaction region in between. We want to describe the scattering process between $\hat{\mathbf{r}}_{(\text{in})}$ and $\hat{\mathbf{r}}_{(\text{out})}$. In this paper we restrict attention to systems whose Hamiltonians are quadratic in the canonical variables $\hat{\mathbf{r}}$. Hence, the equations of motion are linear and, consequently, the in and out modes are related by a simple matrix multiplication:

$$\hat{\mathbf{r}}_{(\text{out})} = \mathbf{S} \cdot \hat{\mathbf{r}}_{(\text{in})}, \tag{B3}$$

where $\mathbf{S}$ is the scattering matrix. As shown below, this matrix can be obtained by solving the classical equations of motion (or equivalently, it can be constructed from the Bogoliubov coefficients). Since the time evolution of a closed system is a canonical transformation, $\mathbf{S}$ must leave the symplectic form invariant, $\mathbf{S} \cdot \mathbf{\Omega} \cdot \mathbf{S}^\top = \mathbf{\Omega}$. In other words, $\mathbf{S}$ must belong to the symplectic group, $\mathbf{S} \in \text{Sp}(\mathbb{R}, 2N)$.

The scattering process can be equivalently formulated using annihilation and creation variables, instead of canonical operators. Define, for each canonical pair $(\hat{x}_I, \hat{p}_I)$, the non-Hermitian operator $\hat{a}_I = \frac{1}{\sqrt{2}}(\hat{x}_I + i\hat{p}_I)$. If we define the vector

$$\hat{\mathbf{A}} \equiv (\hat{a}_1, \hat{a}_1^\dagger, \cdots, \hat{a}_N, \hat{a}_N^\dagger), \tag{B4}$$

then the relation between $\hat{\mathbf{r}}$ and $\hat{\mathbf{A}}$ reads

$$\hat{\mathbf{A}} = \mathbf{B} \cdot \hat{\mathbf{r}}, \quad \mathbf{B} \equiv \bigoplus_N \frac{1}{\sqrt{2}} \begin{pmatrix} 1 & i \\ 1 & -i \end{pmatrix}, \tag{B5}$$

where we have denoted by $\mathbf{B}$ the "change of basis" matrix between $\hat{\mathbf{A}}$ and $\hat{\mathbf{r}}$. In these variables, the canonical commutation relations read

$$[\hat{\mathbf{A}}, \hat{\mathbf{A}}] = \mathbf{B}\,[\hat{\mathbf{r}}, \hat{\mathbf{r}}]\,\mathbf{B}^{-1} = \mathbf{B}\,i\,\mathbf{\Omega}\,\mathbf{B}^\top = \mathbf{\Omega}.$$

This expression compactly captures the familiar commutation relation of annihilation and creation operators.

The scattering matrix between in and out modes can now be written as

$$\hat{\mathbf{A}}_{(\text{out})} = \mathbf{S}_{(\mathbf{A})} \cdot \hat{\mathbf{A}}_{(\text{in})}, \tag{B6}$$

where $\mathbf{S}_{(\mathbf{A})}$ is related to $\mathbf{S}_{(\mathbf{r})}$ by $\mathbf{S}_{(\mathbf{A})} = \mathbf{B} \cdot \mathbf{S}_{(\mathbf{r})} \cdot \mathbf{B}^{-1}$. It is common to refer to the components of $\mathbf{S}_{(\mathbf{A})}$ as Bogoliubov coefficients α_{IJ} and β_{IJ}:

$$\mathbf{S}_{(\mathbf{A})} \equiv \begin{bmatrix} \alpha_{11} & \beta_{11}^* & \cdots & \alpha_{1N} & \beta_{1N}^* \\ \beta_{11} & \alpha_{11}^* & \cdots & \beta_{1N} & \alpha_{1N}^* \\ \vdots & \vdots & \vdots & \vdots & \vdots \\ \alpha_{N1} & \beta_{N1}^* & \cdots & \alpha_{NN} & \beta_{NN}^* \\ \beta_{N1} & \alpha_{N1}^* & \cdots & \beta_{NN} & \alpha_{NN}^* \end{bmatrix}. \tag{B7}$$

The matrix $\mathbf{S}_{(\mathbf{A})}$ also belongs to the symplectic group. The property $\mathbf{S}_{(\mathbf{A})} \cdot \mathbf{\Omega} \cdot \mathbf{S}_{(\mathbf{A})}^\top = \mathbf{\Omega}$ is equivalent to the perhaps more familiar constraints satisfied by Bogoliubov coefficients:

$$\sum_K (\alpha_{IK}\alpha_{JK}^* - \beta_{IK}^*\beta_{JK}) = \delta_{IJ},$$
$$\sum_K (\alpha_{IK}\beta_{JK}^* - \alpha_{IK}\beta_{JK}^*) = 0. \tag{B8}$$

2. Gaussian states

We restrict our analyses to Gaussian states. Recall that Gaussian states $\hat{\rho}$, pure or mixed, are quantum states for which the quantum moments $\langle \hat{\mathbf{r}}^{i_1} \cdots \hat{\mathbf{r}}^{i_n} \rangle$ satisfy the same relations as the statistical moments of a Gaussian multivariable probability distribution. This implies, in particular, that the first and second moments completely determine the rest. Therefore, rather than working with the density matrix $\hat{\rho}$, which is infinite dimensional, one can alternatively describe in full a Gaussian state by the $2N$ dimensional vector of its first moments

$$\boldsymbol{\mu} = \langle \hat{\mathbf{r}} \rangle, \tag{B9}$$

and its symmetrized second moments (the so-called covariance matrix)

$$\boldsymbol{\sigma} = \langle \{(\hat{\mathbf{r}} - \boldsymbol{\mu}), (\hat{\mathbf{r}} - \boldsymbol{\mu})\} \rangle, \tag{B10}$$

where the curly brackets denote the anticommutator.[5]

Gaussian states include vacua, coherent, thermal, and squeezed states. Therefore, although our analysis is restricted, the family of Gaussian states is sufficiently general to describe most of the states one can easily create and manipulate in the laboratory. To give a few examples, the vacuum of a set

[5]One subtracts $\boldsymbol{\mu}$ in the definition of $\boldsymbol{\sigma}$ to avoid having redundant information in the first and second moments. One focuses on the symmetric part of the second moments because the antisymmetric part is determined by the canonical commutation relations, and is state independent. Therefore, the pair $(\boldsymbol{\mu}, \boldsymbol{\sigma})$ is the minimum information needed to completely and uniquely characterize a Gaussian state.

of N oscillators is characterized by $\boldsymbol{\mu} = \mathbf{0}$, $\boldsymbol{\sigma} = \boldsymbol{I}_{2N}$; a coherent state is characterized by $\boldsymbol{\mu} \neq \mathbf{0}$, $\boldsymbol{\sigma} = \boldsymbol{I}_{2N}$; and a thermal state is characterized by $\boldsymbol{\mu} = \mathbf{0}$, $\boldsymbol{\sigma} = \bigoplus_I (1 + 2n_I)\boldsymbol{I}_2$, where n_I is the mean number of thermal quanta in the mode $I = 1, \cdots, N$. Thermal states are mixed Gaussian states.

Many properties of a Gaussian state can be extracted easily from $\boldsymbol{\sigma}$. One such property that we use in the main body of this paper is the purity P. It is obtained from the covariance matrix of the Gaussian state by $P(\sigma) = 1/\sqrt{\det\sigma}$; it is 1 for pure states and smaller than 1 for mixed states. Note the purity does not depend on the first moments.

Evolving Gaussian states under quadratic Hamiltonians is very simple. The linearity of the evolution guarantees that an initial Gaussian state $(\boldsymbol{\mu}^{(\text{in})}, \boldsymbol{\sigma}^{(\text{in})})$ evolves to another Gaussian state $(\boldsymbol{\mu}^{(\text{out})}, \boldsymbol{\sigma}^{(\text{out})})$ determined by

$$\boldsymbol{\mu}^{(\text{out})} = \boldsymbol{S}\boldsymbol{\mu}^{(\text{in})}, \tag{B11}$$

$$\boldsymbol{\sigma}^{(\text{out})} = \boldsymbol{S}\boldsymbol{\sigma}^{(\text{in})}\boldsymbol{S}^{\top}. \tag{B12}$$

3. Entanglement in Gaussian states

Consider a partition of the system of N modes in two subsystems, each made of a subset of the canonical pairs $(\hat{x}_I, \hat{p}_I)$ (these are Gaussian subsystems). The first moments and covariance matrix of a Gaussian state for the entire system have the following form:

$$\boldsymbol{\mu}_{AB} = (\boldsymbol{\mu}_A, \boldsymbol{\mu}_B)^{\top}, \tag{B13}$$

$$\boldsymbol{\sigma}_{AB} = \begin{bmatrix} \boldsymbol{\sigma}_A^{(\text{red})} & \mathbf{C}_{AB} \\ \mathbf{C}_{AB}^{\top} & \boldsymbol{\sigma}_B^{(\text{red})} \end{bmatrix} \tag{B14}$$

where $(\boldsymbol{\mu}_A, \boldsymbol{\sigma}_A^{(\text{red})})$ and $(\boldsymbol{\mu}_B, \boldsymbol{\sigma}_B^{(\text{red})})$ describe the reduced Gaussian state of each subsystem individually. The matrix $\mathbf{C}_{AB}$ describes the correlations between the two subsystems; these correlations could be classical or contain entanglement.

If the total state is pure, the von Neumann entropies of the reduced state of each of the subsystems are equal to each other, and it provides a faithful quantifier entanglement between A and B—the so-called entanglement entropy. The von Neumann entropy of a Gaussian state $(\boldsymbol{\mu}, \boldsymbol{\sigma})$ for an N-mode system can be easily computed from the N symplectic eigenvalues of $\boldsymbol{\sigma}$, denoted by ν_I, with $I = 1 \cdots N$. The symplectic eigenvalues are equal to the modulus of the eigenvalues of the matrix $\boldsymbol{\sigma}^{ik}\boldsymbol{\Omega}^{-1}_{kj}$. The von Neumann entropy reads

$$S[\boldsymbol{\sigma}] = \sum_I^N \left[\left(\frac{\nu_I + 1}{2}\right) \log_2 \left(\frac{\nu_I + 1}{2}\right) \right. \tag{B15}$$

$$\left. - \left(\frac{\nu_I - 1}{2}\right) \log_2 \left(\frac{\nu_I - 1}{2}\right) \right]. \tag{B16}$$

If the total state is mixed, the von Neumann entropy of the subsystems is no longer an entanglement measure. A convenient measure for pure and mixed states alike is the logarithmic negativity, $E_{\mathcal{N}}$. The logarithmic negativity is in one-to-one correspondence with the violation of the PPT criterion for quantum states [47–49], a criterion that all separable quantum states obey. For a Gaussian state made of two Gaussian subsystems A and B, it is given by

$$E_{\mathcal{N}}[\boldsymbol{\sigma}] = \sum_I \max[0, -\log_2 \tilde{\nu}_I], \tag{B17}$$

where $\tilde{\nu}_I$ are the symplectic eigenvalues of the *partially transposed* covariance matrix $\tilde{\boldsymbol{\sigma}}$, defined from $\boldsymbol{\sigma}$ by reversing the sign of all components involving one momenta $\hat{p}_I$ of the subsystem B. If either of the Gaussian subsystems is made of a single mode, $(N_A = 1)$, regardless of the size of the other subsystem, $E_{\mathcal{N}}$ is a faithful entanglement quantifier, in the sense that $E_{\mathcal{N}} = 0$ if and only if the state is separable. It is also an entanglement monotone, and hence it can be used to quantify entanglement (see Ref. [46] for further details). For Gaussian quantum states, the value of the $E_{\mathcal{N}}$ has an operational meaning as the exact cost (measured in "Bell pairs" or ebits) that is required to prepare or simulate the quantum state under consideration [59,60].

In the analog gravity literature, there has been focus on a particular Cauchy-Schwarz inequality to evaluate entanglement between two single-mode systems in a state $\hat{\rho}_{AB}$, first introduced in Refs. [61] and further discussed in Refs. [62,63] (see also Ref. [64]). Consider the quantity

$$\Delta \equiv \langle \hat{n}_A \rangle \langle \hat{n}_B \rangle - |\langle \hat{a}_A \hat{a}_B \rangle|^2, \tag{B18}$$

where $\hat{a}_A$ and $\hat{a}_B$ are annihilation operators for each mode, and $\hat{n}_A$ and $\hat{n}_B$ are number operators defined from them, respectively. The inequality $\Delta < 0$ is a *sufficient* condition for entanglement. It is not necessary though, in the sense that some entangled states do not violate the inequality. It is not an entanglement monotone either [40], even when restricted to Gaussian states. But it is a useful criterion to signal the presence of entanglement in many circumstances, particularly convenient because its evaluation requires only knowledge of three moments $\langle \hat{n}_A \rangle$, $\langle \hat{n}_B \rangle$, and $\langle \hat{a}_A \hat{a}_B \rangle$. In contrast, $E_{\mathcal{N}}$ requires knowledge of the entire covariance matrix, something that demands full state tomography on the two-mode system.

APPENDIX C: THE CASE OF A C^2 SCALE FACTOR

In this Appendix, we describe the expanding toroidal BEC dynamics with a C^2 scale factor which describes asymptotically static regions in the past and future with an inflationary phase in between. I.e., we study $a(t)$ that is continuous and also has continuous first and second time derivatives. This was studied analytically by Glenz and Parker [45] for the case of a scalar field in a $(3 + 1)$-dimensional spacetime.

As discussed in the main text, scalar modes χ_k in the expanding toroidal BEC evolve on an analog FLRW background characterized by scale factor $a(t)$ and satisfy the Mukhanov-Sasaki equation [42–44]:

$$\ddot{\chi}_k + (1 + \gamma)\frac{\dot{a}}{a}\dot{\chi}_k + \frac{k^2}{a^2}\chi_k = 0, \tag{C1}$$

which can be derived from Eq. (4) by setting $\alpha = 1$, substituting $R(t) = R_0 a(t)$, and defining the wave number $k = nc/R_0$ in terms of the mode index. The entire evolution of the scale

factor consists of three regimes:

$$a(t) = \begin{cases} a_i(t), & \text{for } t < t_1, \\ a_{\rm inf}(t), & \text{for } t_1 \leqslant t \leqslant t_2, \\ a_f(t), & \text{for } t > t_2, \end{cases} \tag{C2}$$

where $a_{\rm inf}(t)$ is an exponential function in proper time and the functions $a_i(t)$ and $a_f(t)$ are asymptotically constant in the future and past, and match (in a C^2 manner) with $a_{\rm inf}(t)$ at times t_1 and t_2, respectively. To write explicit forms for these functions, it is convenient to switch to the harmonic time variable τ, defined in terms of proper time t by $d\tau = a(t)^{-(1+\gamma)}dt$. We emphasize that this is distinct from the parameter τ used in the main text to define the Hubble timescale.

The initial regime (denoted by subscript i) has the following smooth scale factor:

$$a_i(\tau) = \left[a_{1i}^{2\gamma} + \left(a_{2i}^{2\gamma} - a_{1i}^{2\gamma}\right) n_{\rm F}(-\tau/s_i)\right]^{\frac{1}{2\gamma}}, \tag{C3}$$

where $n_{\rm F}(x) = (e^x + 1)^{-1}$ is the Fermi-Dirac function. The above scale factor approaches a_{1i} at early times ($\tau \to -\infty$) and approaches a_{2i} at late times ($\tau \to \infty$), with s_i the timescale associated with this initial regime. Then, at some time t_1, an inflationary regime sets in where the scale factor is given by an exponential in proper time:

$$a_{\rm inf}(t) = a(t_1) e^{H_{\rm inf}(t-t_1)}, \tag{C4}$$

where $H_{\rm inf}$ is the constant Hubble parameter whose inverse determines the timescale of the expansion. To achieve C^2, we demand that at $t = t_1$ the scale factors a_i and $a_{\rm inf}$ are equal, and that the maximum value of the Hubble parameter $H(t) = a^{-1}da/dt$ of the first regime equals $H_{\rm inf}$ (ensuring continuity of the first and second derivatives). This helps us obtain the time $\tau_i = \tau_i(t_1)$ at which the first regime smoothly joins onto the inflationary regime:

$$\tau_i = s_i \log \frac{(1+\gamma)\left(a_{1i}^{2\gamma} - a_{2i}^{2\gamma}\right) + C_i}{4\gamma a_{2i}^{2\gamma}}. \tag{C5}$$

From this, we obtain the scale factor $a(t_1)$ at t_1 [see Eq. (C4)]:

$$a(\tau_i) = a(t_1) = \left[\frac{-(1+\gamma)\left(a_{1i}^{2\gamma} + a_{2i}^{2\gamma}\right) + C_i}{2(-1+\gamma)}\right]^{\frac{1}{2\gamma}}. \tag{C6}$$

Lastly, by equating the Hubble rate $H(t)$ at the junction $t = t_1$, we find the Hubble parameter $H_{\rm inf}$ during inflation to be

$$H_{\rm inf} = \frac{[-2\gamma\left(a_{1i}^{2\gamma} + a_{2i}^{2\gamma}\right) + C_i]}{\left(a_{1i}^{2\gamma} - a_{2i}^{2\gamma}\right) s_i(-1+\gamma)(1+3\gamma)} \times \left[\frac{-(1+\gamma)\left(a_{1i}^{2\gamma} + a_{2i}^{2\gamma}\right) + C_i}{2(-1+\gamma)}\right]^{-\frac{(1+\gamma)}{2\gamma}}. \tag{C7}$$

In all these expressions, i.e., Eqs. (C5)–(C7), we used the function C_i which is defined as follows:

$$C_i = \sqrt{(1+\gamma)^2 a_{1i}^{4\gamma} + (14\gamma^2 - 4\gamma - 2)^2 a_{1i}^{2\gamma} a_{2i}^{2\gamma} + (1+\gamma)^2 a_{2i}^{4\gamma}}. \tag{C8}$$

The preceding steps ensure that the first two regimes of Eq. (C2) match in a C^2 manner at t_1. Now, we repeat these steps at time $t = t_2$, where inflation ends and the final regime begins (denoted by subscript f). We take the final regime scale factor to have a form similar to Eq. (C3):

$$a_f(\tau') = \left[a_{1f}^{2\gamma} + \left(a_{2f}^{2\gamma} - a_{1f}^{2\gamma}\right) n_{\rm F}(-\tau'/s_f)\right]^{\frac{1}{2\gamma}}, \tag{C9}$$

but with the replacement $i \to f$, and using a different time variable τ' for this regime. Again demanding the continuity of the scale factors $a_f(\tau')$ and $a_{\rm inf}(t)$ at $t = t_2$ (equivalent to $\tau' = \tau'_f$), we obtain the timescale of the final regime as $s_f = s_i(i \to f)$, and the joining time to be $\tau'_f = \tau_i(i \to f)$ [obtained by replacing $i \to f$ in Eq. (C5)]. It is convenient to express these results in terms of the number of e foldings N that is defined to be logarithm of the ratio of the final scale factor and initial scale factor. Thus we write the following:

$$a_{2i} = a_{1i} e^{N_i}, \quad a_{2f} = a_{2i}\, e^{N_{\rm inf} + N_f}. \tag{C10}$$

In addition to this, if we also assume that the initial scale factor in the remote past is unity, i.e., $a_{1i} = 1$, then we end up with four independent variables—N_i, s_i, $N_{\rm inf}$, and N_f—that characterize the C^2 scale factor (C2) for the inflationary toroidal BEC. Our next task is to solve Eq. (C1) in all three regimes, matching the solutions.

To do this, it is convenient to rewrite the Mukhanov-Sasaki equation (C1) in terms of harmonic time as follows:

$$\chi_k'' + k^2 a^{2\gamma} \chi_k = 0, \tag{C11}$$

where the prime symbol denotes differentiation with respect to the harmonic time τ. For the initial regime (C3), the general solution to (C11) is a linear combination of hypergeometric functions ${}_2F_1(a, b; c; d)$:

$$\begin{aligned} \chi_k(\tau) &= \frac{\delta_1(k)}{\sqrt{2ka_{1i}^{\gamma}}} e^{-ia_{1i}^{\gamma} k\tau}\, {}_2F_1(-a_i + b_i, -a_i - b_i; 1 - 2a_i; -e^{\tau/s_i}) \\ &\quad + \frac{\delta_2(k)}{\sqrt{2ka_{1i}^{\gamma}}} e^{-ia_{1i}^{\gamma} k\tau}\, {}_2F_1(a_i + b_i, a_i - b_i; 1 + 2a_i; -e^{\tau/s_i}), \end{aligned} \tag{C12}$$

where $\delta_{1,2}(k)$ are coefficients that are fixed by imposing initial conditions on the modes, $a_i = ika_{1i}^{\gamma} s_i$ and $b_i = ika_{2i}^{\gamma} s_i$. Assuming that the modes are in a vacuum state at early times $\tau \to -\infty$, we can take them to consist of only positive-frequency plane-wave solutions:

$$\lim_{\tau \to -\infty} \chi_k(\tau) = \frac{1}{\sqrt{2ka_{1i}^{\gamma}}} e^{-ia_{1i}^{\gamma} k\tau}. \tag{C13}$$

This condition helps us pick out the correct form of the mode functions in the initial regime to be

$$\chi_k(\tau) = \frac{1}{\sqrt{2ka_{1i}^{\gamma}}} e^{-ia_{1i}^{\gamma}k\tau}\, {}_2F_1(-a_i + b_i, -a_i - b_i; 1 - 2a_i; -e^{\tau/s_i}). \tag{C14}$$

In the inflationary regime with the exponential scale factor (C4), the Mukhanov-Sasaki equation yields the following mode solution:

$$\chi_k(t) = \frac{i}{2}\sqrt{\frac{\pi}{H_{\rm inf}}}\, a_{\rm inf}^{-\frac{1+\gamma}{2}}(t)\left[E(k)H^{(1)}_{\frac{1+\gamma}{2}}\left(\frac{k}{a_{\rm inf}(t)H_{\rm inf}}\right) - F(k)H^{(2)}_{\frac{1+\gamma}{2}}\left(\frac{k}{a_{\rm inf}(t)H_{\rm inf}}\right)\right],$$

where $H^{(1)}$ and $H^{(2)}$ are Hankel functions of first and second kind, respectively, and the coefficients $E(k)$ and $F(k)$ are fixed by matching the modes and their first derivatives at $t = t_1$. Finally, the solution to Mukhanov-Sasaki equation in the final regime (C9) is similar to (C12) but with $i \to f$:

$$\begin{aligned}\chi_k(\tau') = {} & \frac{C(k)}{\sqrt{2ka_{1f}^{\gamma}}} e^{-ia_{1f}^{\gamma}k\tau'}\, {}_2F_1(-a_f + b_f, -a_f - b_f; 1 - 2a_f; -e^{\tau'/s_f}) \\ & + \frac{D(k)}{\sqrt{2ka_{1f}^{\gamma}}} e^{ia_{1f}^{\gamma}k\tau'}\, {}_2F_1(a_f + b_f, a_f - b_f; 1 + 2a_f; -e^{\tau'/s_f}),\end{aligned} \tag{C15}$$

where $a_f = ika_{1f}^{\gamma}s_f$ and $b_f = ika_{2f}^{\gamma}s_f$, and the coefficients $C(k)$ and $D(k)$ are fixed by matching the mode functions and their first time derivatives at $t = t_2$. At late times, the scale factor (C9) approaches the constant value a_{2f}, and thus we expect that the modes behave as a linear combination of positive and negative frequency plane waves:

$$\lim_{\tau\to\infty} \chi_k(\tau') \sim \frac{1}{\sqrt{2ka_{2f}^{\gamma}}}\left(\alpha_k e^{-ia_{2f}^{\gamma}k\tau'} + \beta_k e^{ia_{2f}^{\gamma}k\tau'}\right), \tag{C16}$$

where α_k and β_k are the Bogoliubov coefficients that satisfy $|\alpha_k|^2 - |\beta_k|^2 = 1$. Following the steps in Ref. [45], we get the following expressions for the Bogoliubov coefficients:

$$\alpha_k = \left(\frac{a_{2f}}{a_{1f}}\right)^{\gamma/2}[C(k)B(k) + D(k)B_t(k)], \tag{C17}$$

$$\beta_k = \left(\frac{a_{2f}}{a_{1f}}\right)^{\gamma/2}[C(k)A(k) + D(k)A_t(k)], \tag{C18}$$

where we define the following functions:

$$\begin{aligned}A(k) &= \frac{\Gamma(1 - 2a_f)\Gamma(2b_f)}{\Gamma(-a_f + b_f)\Gamma(1 - a_f + b_f)}, \\ B(k) &= \frac{\Gamma(1 - 2a_f)\Gamma(-2b_f)}{\Gamma(-a_f - b_f)\Gamma(1 - a_f - b_f)},\end{aligned} \tag{C19}$$

and the other two functions are related to these via $A_t(k) = A(k)[a_f \to -a_f]$ and $B_t(k) = A(k)[b_f \to -b_f]$.

The preceding equations determine the particle creation number $|\beta_k|^2$ for an inflationary toroidal BEC undergoing an expansion that is C^2 everywhere with a exponential ("de Sitter"-like) central regime. Next, we show that this particle creation exhibits a universal behavior reflecting intrinsic properties of the inflation (such as the damping parameter γ). To do this, in Fig. 11, we show a log-log plot of the particle creation probability $|\beta_k|^2$ vs the normalized wave number q defined as follows:

$$q = \frac{k}{\sqrt{\frac{\gamma}{2} + \frac{\gamma^2}{4}}H_{\rm inf}a_f(\tau_f')}. \tag{C20}$$

To focus on inflationary physics, we chose the number of e foldings to be small in the initial and final regimes [$N_i = N_f = \log(1.1)$] and large in the de Sitter regime ($N_{\rm inf} = 20$). Figure 11 shows that there exists an intermediate regime of wave numbers for which the modes only experience the inflationary expansion with the particle creation spectrum showing

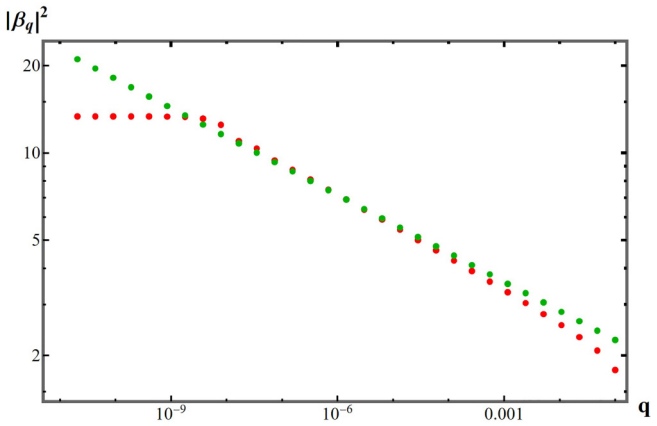

FIG. 11. Log-log plot of particle creation number $|\beta_q|^2$ vs the normalized wave number q (red circles). For small wave numbers, $|\beta_q|^2$ is constant, for intermediate wave numbers it shows a universal linear behavior due to inflation, and for large wave numbers it rapidly decays. In the linear inflationary regime, $|\beta_q|^2 \sim q^{-\gamma}$ and thus the slope of the log-log plot is γ (green circles, which decay exactly as $q^{-\gamma}$, have been added for comparison). For this plot, and without loss of generality, we take in the initial regime the scale factor to be $a_{1i} = 1$, number of e folds $N_i = \log(1.1)$, and timescale for expansion $s_i = 1$. We chose the inflationary regime to have a large number of e folds $N_{\rm inf} = 20$, whereas for the final regime we took $N_f = \log(1.1)$, and we chose the quantum pressure to be $\gamma = 0.1$.

the power-law behavior:

$$|\beta_q|^2 \sim q^{-\gamma}, \tag{C21}$$

that reflects the damping parameter γ. This is precisely what is expected from an analysis of the asymptotic behavior of the Hankel function $H^{(1)}_{\frac{1+\gamma}{2}}$. Thus, the particle-production spectrum in a expanding toroidal BEC indeed shows universal behavior due to inflation when the scale factor is C^2 [45].

Note that in the main text we have focused on a C^0 expansion; i.e., the radius $R(t)$ [or the scale factor $a(t)$] is continuous, but its derivatives are not. In such cases, we get a different power law $|\beta_q|^2 \sim q^{-2}$ at asymptotically large mode wave vector [see Eq. (10)] with the power law $|\beta_q|^2 \sim q^{-\gamma}$ holding at intermediate wave vectors [see Eq. (11)]. In addition, the C^0 case exhibits oscillations. One might ask whether the C^2 case with insignificant initial and final regimes (i.e., N_i, s_i, N_f, and s_f are all very small) is able to reproduce these features of the C^0 case. We find that in this limit, $|\beta_q|^2$ pertaining to the C^2 case indeed starts exhibiting oscillations, but its overall magnitude and power law with respect to the mode index do not agree with the C^0 case. Thus some of the features of the C^0 case are not rooted entirely in the inflationary regime, and some of them result just from the C^0 character of $R(t)$ (a discontinuity in the derivative), i.e., they would not appear for any smooth $R(t)$. In the laboratory, any $R(t)$ that one can create is smooth, and in this sense some of the features of the C^0 could be called mathematical artifacts. On the other hand, the C^0 expansion has advantages in that it allows us to solve for the β coefficients analytically. Additionally, even though the C^2 case more plausibly avoids such artifacts, the universal linear feature due to inflation only appears in the limit of large number of inflationary e foldings, which might not be possible to achieve in a real experiment.

In any case, the formulas developed in this paper apply equally well to all expansion histories that are time independent in the past and future.

[1] L. Parker, *The Creation of Particles in an Expanding Universe*, Ph.D. thesis, Harvard University, 1966.

[2] L. Parker, Particle creation in expanding universes, Phys. Rev. Lett. **21**, 562 (1968).

[3] E. Schrödinger, The proper vibrations of the expanding universe, Physica **6**, 899 (1939).

[4] S. W. Hawking, Black hole explosions, Nature (London) **248**, 30 (1974).

[5] S. W. Hawking, Particle creation by black holes, Commun. Math. Phys. **43**, 199 (1975); **46**, 206 (1976).

[6] A. A. Starobinsky, A new type of isotropic cosmological models without singularity, Phys. Lett. B **91**, 99 (1980).

[7] A. H. Guth, Inflationary universe: A possible solution to the horizon and flatness problems, Phys. Rev. D **23**, 347 (1981).

[8] A. Albrecht and P. J. Steinhardt, Cosmology for grand unified theories with radiatively induced symmetry breaking, Phys. Rev. Lett. **48**, 1220 (1982).

[9] S. W. Hawking and I. G. Moss, Supercooled phase transitions in the very early universe, Phys. Lett. B **110**, 35 (1982).

[10] A. D. Linde, A new inflationary universe scenario: A possible solution of the horizon, flatness, homogeneity, isotropy and primordial monopole problems, Phys. Lett. B **108**, 389 (1982).

[11] A. D. Linde, Chaotic inflation, Phys. Lett. B **129**, 177 (1983).

[12] A. R. Liddle and D. H. Lyth, *Cosmological Inflation and Large Scale Structure* (Cambridge University, New York, 2000).

[13] R. de Putter and O. Doré, In search of an observational quantum signature of the primordial perturbations in slow-roll and ultraslow-roll inflation, Phys. Rev. D **101**, 043511 (2020).

[14] J. Martin and V. Vennin, Quantum discord of cosmic inflation: Can we show that CMB anisotropies are of quantum-mechanical origin? Phys. Rev. D **93**, 023505 (2016).

[15] J. Martin and V. Vennin, Obstructions to Bell CMB experiments, Phys. Rev. D **96**, 063501 (2017).

[16] D. Campo and R. Parentani, Inflationary spectra and violations of Bell inequalities, Phys. Rev. D **74**, 025001 (2006).

[17] J. Maldacena, A model with cosmological Bell inequalities, Fortschr. Phys. **64**, 10 (2016).

[18] S. Kanno and J. Soda, Infinite violation of Bell inequalities in inflation, Phys. Rev. D **96**, 083501 (2017).

[19] S. Choudhury, S. Panda, and R. Singh, Bell violation in the Sky, Eur. Phys. J. C **77**, 60 (2017).

[20] J. Martin and V. Vennin, Real-space entanglement in the cosmic microwave background, J. Cosmol. Astropart. Phys. **10**, 036 (2021).

[21] I. Agullo, B. Bonga, and P. R. Metidieri, Does inflation squeeze cosmological perturbations? J. Cosmol. Astropart. Phys. **9**, 032 (2022).

[22] J. T. Hsiang and B. L. Hu, No intrinsic decoherence of inflationary cosmological perturbations, Universe **8**, 27 (2022).

[23] E. Martín-Martínez and N. C. Menicucci, Cosmological quantum entanglement, Class. Quantum Grav. **29**, 224003 (2012).

[24] I. Fuentes, R. B. Mann, E. Martín-Martínez, and S. Moradi, Entanglement of Dirac fields in an expanding spacetime, Phys. Rev. D **82**, 045030 (2010).

[25] W. G. Unruh, Experimental black hole evaporation, Phys. Rev. Lett. **46**, 1351 (1981).

[26] C. Barcelo, S. Liberati, and M. Visser, Analogue gravity, Living Rev. Rel. **14**, 3 (2011).

[27] S. Eckel, A. Kumar, T. Jacobson, I. B. Spielman, and G. K. Campbell, A rapidly expanding Bose-Einstein condensate: an expanding universe in the lab, Phys. Rev. X **8**, 021021 (2018).

[28] S. Banik, M. Gutierrez Galan, H. Sosa-Martinez, M. Anderson, S. Eckel, I. B. Spielman, and G. K. Campbell, Accurate determination of Hubble attenuation and amplification in expanding and contracting cold-atom universes, Phys. Rev. Lett. **128**, 090401 (2022).

[29] J. M. Gomez Llorente and J. Plata, Expanding ring-shaped Bose-Einstein condensates as analogs of cosmological models: Analytical characterization of the inflationary dynamics, Phys. Rev. A **100**, 043613 (2019).

[30] A. Bhardwaj, D. Vaido, and D. E. Sheehy, Inflationary dynamics and particle production in a toroidal Bose-Einstein condensate, Phys. Rev. A **103**, 023322 (2021).
[31] S. Eckel and T. Jacobson, Phonon redshift and Hubble friction in an expanding BEC, SciPost Phys. **10**, 064 (2021).
[32] A. Einstein, B. Podolsky, and N. Rosen, Can quantum mechanical description of physical reality be considered complete? Phys. Rev. **47**, 777 (1935).
[33] Z. Y. Ou and L. Mandel, Violation of Bell's inequality and classical probability in a two-photon correlation experiment, Phys. Rev. Lett. **61**, 50 (1988).
[34] Y. H. Shih and C. O. Alley, New type of einstein-Podolsky-Rosen-Bohm experiment using pairs of light quanta produced by optical parametric down conversion, Phys. Rev. Lett. **61**, 2921 (1988).
[35] A. Aspect, Bell's inequality test: More ideal than ever, Nature (London) **398**, 189 (1999).
[36] M. Bonneau, J. Ruaudel, R. Lopes, J.-C. Jaskula, A. Aspect, D. Boiron, and C. I. Westbrook, Tunable source of correlated atom beams, Phys. Rev. A **87**, 061603(R) (2013).
[37] F. Borselli, M. Maiwöger, T. Zhang, P. Haslinger, V. Mukherjee, A. Negretti, S. Montangero, T. Calarco, I. Mazets, M. Bonneau, and J. Schmiedmayer, Two-particle interference with double twin-atom beams, Phys. Rev. Lett. **126**, 083603 (2021).
[38] B. Sundar, D. Barberena, A. Piñeiro Orioli, A. Chu, J. K. Thompson, A. M. Rey, and R. J. Lewis-Swan, Bosonic pair production and squeezing for optical phase measurements in long-lived dipoles coupled to a cavity, Phys. Rev. Lett. **130**, 113202 (2023).
[39] I. Agullo, A. J. Brady, and D. Kranas, Quantum aspects of stimulated hawking radiation in an optical analog white-black hole pair, Phys. Rev. Lett. **128**, 091301 (2022).
[40] A. J. Brady, I. Agullo, and D. Kranas, Symplectic circuits, entanglement, and stimulated Hawking radiation in analogue gravity, Phys. Rev. D **106**, 105021 (2022).
[41] C. J. Pethick and H. Smith, *Bose-Einstein Condensation in Dilute Gases*, 2nd ed. (Cambridge University, New York, 2008).
[42] M. Sasaki, Gauge invariant scalar perturbations in the new inflationary universe, Prog. Theor. Phys. **70**, 394 (1983).
[43] H. Kodama and M. Sasaki, Cosmological perturbation theory, Prog. Theor. Phys. Suppl. **78**, 1 (1984).
[44] V. F. Mukhanov, Quantum theory of gauge invariant cosmological perturbations, Sov. Phys. JETP **67**, 1297 (1988).
[45] M. M. Glenz and L. Parker, Study of the spectrum of inflaton perturbations, Phys. Rev. D **80**, 063534 (2009).
[46] A. Serafini, *Quantum Continuous Variables: A Primer of Theoretical Methods* (CRC, Boca Raton, FL, 2017).
[47] A. Peres, Separability criterion for density matrices, Phys. Rev. Lett. **77**, 1413 (1996).
[48] M. B. Plenio, Logarithmic negativity: A full entanglement monotone that is not convex, Phys. Rev. Lett. **95**, 090503 (2005).
[49] R. Simon, Peres-Horodecki separability criterion for continuous variable systems, Phys. Rev. Lett. **84**, 2726 (2000).
[50] J. K. Asbóth, J. Calsamiglia, and H. Ritsch, Computable measure of nonclassicality for light, Phys. Rev. Lett. **94**, 173602 (2005).
[51] S. L. Braunstein, Squeezing as an irreducible resource, Phys. Rev. A **71**, 055801 (2005).
[52] D. Hellweg, L. Cacciapuoti, M. Kottke, T. Schulte, K. Sengstock, W. Ertmer, and J. J. Arlt, Measurement of the spatial correlation function of phase fluctuating Bose-Einstein condensates, Phys. Rev. Lett. **91**, 010406 (2003).
[53] R. Hanbury Brown and R. Q. Twiss, A new type of interferometer for use in radio astronomy, Philos. Mag. **45**, 663 (1954).
[54] R. Hanbury Brown and R. Q. Twiss, Correlation between photons in two coherent beams of light, Nature (London) **177**, 27 (1956).
[55] R. Hanbury Brown and R. Q. Twiss, A test of a new type of stellar interferometer on Sirius, Nature (London) **178**, 1046 (1956).
[56] M. Tolosa-Simeón, Á. Parra-López, N. Sánchez-Kuntz, T. Haas, C. Viermann, M. Sparn, N. Liebster, M. Hans, E. Kath, and H. Strobel *et al.*, Curved and expanding spacetime geometries in Bose-Einstein condensates, Phys. Rev. A **106**, 033313 (2022).
[57] C. Viermann, M. Sparn, N. Liebster, M. Hans, E. Kath, Á. Parra-López, M. Tolosa-Simeón, N. Sánchez-Kuntz, T. Haas, and H. Strobel *et al.*, Quantum field simulator for dynamics in curved spacetime, Nature (London) **611**, 260 (2022).
[58] C. A. Chen, S. Khlebnikov, and C. L. Hung, Observation of quasiparticle pair production and quantum entanglement in atomic quantum gases quenched to an attractive interaction, Phys. Rev. Lett. **127**, 060404 (2021).
[59] X. Wang and M. M. Wilde, Cost of quantum entanglement simplified, Phys. Rev. Lett. **125**, 040502 (2020).
[60] X. Wang and M. M. Wilde, α-logarithmic negativity, Phys. Rev. A **102**, 032416 (2020).
[61] J. R. M. de Nova, F. Sols, and I. Zapata, Violation of Cauchy-Schwarz inequalities by spontaneous Hawking radiation in resonant boson structures, Phys. Rev. A **89**, 043808 (2014).
[62] X. Busch, I. Carusotto, and R. Parentani, Spectrum and entanglement of phonons in quantum fluids of light, Phys. Rev. A **89**, 043819 (2014).
[63] X. Busch and R. Parentani, Quantum entanglement in analogue Hawking radiation: When is the final state nonseparable? Phys. Rev. D **89**, 105024 (2014).
[64] T. Wasak, P. Szańkowski, P. Ziń, M. Trippenbach, and J. Chwedeńczuk, Cauchy-Schwarz inequality and particle entanglement, Phys. Rev. A **90**, 033616 (2014).